$P = 0.79$]).[47] Two other phase III, randomized, placebo-controlled trials evaluating the efficacy of sorafenib in combination with conventional TACE are ongoing (NCT01004978 and NCT01324076).

Other phase III RCT exploring the combinations of TACE and orantinib (ORIENTAL trial, NCT01465464) and brivanib (BRISK-TA trial) have been completed, and sunitinib (TURNE trial, NCT01164202) are ongoing.

In the BRISK-TA trial, although brivanib improved time to radiographic progression (brivanib vs placebo; 8.4 vs 4.9 months; HR, 0.61; 95% CI, 0.48–0.77; $P < 0.0001$), brivanib did not improve TTP (brivanib vs placebo; 12.0 vs 10.9 months; HR, 0.94; 95% CI, 0.72–1.22; $P = 0.62$) or OS (brivanib vs placebo; 26.4 vs 26.1 months; HR, 0.90; 95% CI, 0.66–1.23; $P = 0.53$).[48]

Orantinib is an oral small molecule inhibitor of VEGFR, PDGFR and FGFR.[49] A recent press release announced that a phase III trial comparing TACE plus orantinib versus TACE plus placebo did not meet the primary end-point, but the full dataset has not yet been reported.

A phase III study of sorafenib plus low-dose cisplatin/fluorouracil HAIC versus sorafenib in patients with advanced HCC is ongoing (NCT01214343).

Biomarkers

Studies have investigated whether several biomarker can predict the response to sorafenib. Tissue markers, such as FGF3/FGF4,[50] αB-crystallin,[51] c-Jun N-terminal kinase,[52] VEGF-A[53] and pERK,[54] serum marker and angiogenesis-related cytokine have been reported.[55] Conventional tumor markers for the diagnosis of HCC, namely, des-γ-carboxyprothrombin and α-fetoprotein, have been reported to show contrasting behavior after administration of sorafenib.[56–60] However, no definitive biomarker for sorafenib has been identified. Lovelt *et al.* reported that no biomarker was significantly associated with the response to sorafenib within the SHARP study, which was the largest study of sorafenib.[61] The difficulty in identifying a specific biomarker in sorafenib therapy for HCC may be due to the presence of multiple molecular targets.

FUTURE DIRECTIONS

NINE PHASE III clinical trials (i.e. SHARP, Asia–Pacific, SUN 1170, BRISK-FL, 0100953, SEARCH, BRISK-PS, EVOLVE-1, REACH) of patients with advanced HCC have been completed, and four phase III clinical trials (i.e. E7080, RESORCE, JET-HCC, CELESTIAL) are ongoing. No targeted agent or regimens other than sorafenib significantly improve OS in patients with advanced HCC, according to phase III trials in the first- or second-line setting. Three phase III clinical trials did not demonstrate any benefit with combination therapy.

Potential reasons for negative results include heterogeneous patient population and the lack of understanding of critical drivers of tumor progression/dissemination. Other reasons include liver toxicity, flaws in trial design or marginal antitumoral efficacy of the agents. When dissecting the results of recent trials,[30–34] we can speculate that the main shortcomings for sunitinib are liver toxicity and issues with trial design.[30] Other shortcomings include lack of efficacy for erlotinib,[34] toxicity for linifanib[33] and lack of efficacy and issues with trial design for brivanib.[31,32]

Hepatocellular carcinoma is a heterogeneous disease, both in regard to its clinical manifestations with underlying liver disease, and its complex pathogenesis involving aberrant signaling in several molecular pathways. Advances in targeted therapy for HCC require a better understanding of various molecular events driving the progression of HCC as well as identification of biomarkers to predict treatment response to targeted agents. Due to the complexity of the mechanisms involved in progression of HCC, the establishment of personalized therapy will require the identification of tissue biomarkers in HCC.

Regarding patient selection, recommendations emphasized the need for standardization of inclusion criteria based on stage, such as the BCLC classification. It is evident that the population of patients with unresectable HCC consists of a highly heterogeneous group of patients with a wide spectrum of survival, ranging from a few months to longer than 2 years.[62,63] Therefore, it is difficult to precisely estimate the survival of patients during the design of clinical trials that encompass a heterogeneous population. As a result, the staging system is suboptimal in identifying a homogeneous group of patients in terms of prognosis and disease behavior.

In summary, success in the development of targeted agents for HCC relies on concerted efforts of testing of novel agents in clinical trials, advancement of knowledge of the molecular events of HCC, discovery of biomarkers to guide personalized treatment and improvements in patient selection.

ACKNOWLEDGMENTS

THIS STUDY WAS supported by grants from the Ministry of Education, Culture, Sports, Science and

Technology-Japan; Ministry of Health, Labor and Welfare-Japan; and Japan Health Sciences Foundation.

REFERENCES

1 El-Serag HB. Epidemiology of viral hepatitis and hepatocellular carcinoma. *Gastroenterology* 2012; **142**: 1264–73.
2 Belghiti J, Fuks D. Liver resection and transplantation in hepatocellular carcinoma. *Liver Cancer* 2012; **1**: 71–82.
3 European Association for the Study of the Liver, European Organisation for Research and Treatment of Cancer. EASL-EORTC clinical practice guidelines: management of hepatocellular carcinoma. *J Hepatol* 2012; **56**: 908–43.
4 Kim B, Kim S, Park J *et al.* Applicability of BCLC stage for prognostic stratification in comparison with other staging systems: single centre experience from long-term clinical outcomes of 1717 treatment-naïve patients with hepatocellular carcinoma. *Liver Int* 2012; **32**: 1120–7.
5 Llovet JM, Ricci S, Mazzaferro V *et al.* Sorafenib in advanced hepatocellular carcinoma. *N Engl J Med* 2008; **359**: 378–90.
6 Cheng AL, Kang YK, Chen Z *et al.* Efficacy and safety of sorafenib in patients in the Asia-Pacific region with advanced hepatocellular carcinoma: a phase III randomised, double-blind, placebo controlled trial. *Lancet Oncol* 2009; **10**: 25–34.
7 Guichard C, Amaddeo G, Imbeaud S *et al.* Integrated analysis of somatic mutations and focal copy-number changes identifies key genes and pathways in hepatocellular carcinoma. *Nat Genet* 2012; **44**: 694–8.
8 Villanueva A, Llovet JM. Liver cancer 2013: mutational landscape of HCC-the end of the beginning. *Nat Rev Clin Oncol* 2014; **11**: 73–4.
9 Zetter BR. Angiogenesis and tumor metastasis. *Annu Rev Med* 1998; **49**: 407–24.
10 Kumar P, Coltas I, Kumar B *et al.* Bcl-2 protects endothelial cells against gamma-radiation via a Raf-MEK-ERK-survivin signalingpathway that is independent of cytochrome c release. *Cancer Res* 2007; **67**: 1193–202.
11 Graupera M, Guillermet-Guibert J, Foukas L *et al.* Angiogenesis selectively requires the p110alpha isoform of PI3K to controlendothelial cell migration. *Nature* 2008; **453**: 662–6.
12 Schoenleber SJ, Kurtz DM, Talwalkar JA *et al.* Prognostic role of vascular endothelial growth factor in hepatocellular carcinoma: systematic review and meta-analysis. *Br J Cancer* 2009; **100**: 1385–92.
13 Kin M, Sata M, Ueno T *et al.* Basic fibroblast growth factor regulates proliferation and motility of human hepatoma cells by an autocrine mechanism. *J Hepatol* 1997; **27**: 677–87.
14 Tsunoda S, Nakamura T, Sakurai H *et al.* Fibroblast growth factor 2- induced host stroma reaction during initial tumor growth promotes progression of mouse melanoma via vascular endothelial growth factor A-dependent neovascularization. *Cancer Sci* 2007; **98**: 541–8.
15 Jain RK, Booth MF. What brings pericytes to tumor vessels? *J Clin Invest* 2003; **112**: 1134–6.
16 Sugimachi K, Tanaka S, Taguchi K *et al.* Angiopoietin switching regulates angiogenesis and progression of human hepatocellular carcinoma. *J Clin Pathol* 2003; **56**: 854–60.
17 Campbell JS, Hughes SD, Gilbertson DG *et al.* Platelet-derived growth factor C induces liver fibrosis, steatosis, and hepatocellular carcinoma. *Proc Natl Acad Sci U S A* 2005; **102**: 3389–94.
18 Crawford Y, Kasman I, Yu L *et al.* PDGFC mediates the angiogenic and tumorigenic properties of fibroblasts associated with tumors refractory to anti-VEGF treatment. *Cancer Cell* 2009; **15**: 21–34.
19 Lau DT, Luxon BA, Xiao SY *et al.* Intrahepatic gene expression profiles and alpha-smooth muscle actin patterns in hepatitis C virus induced fibrosis. *Hepatology* 2005; **42**: 273–81.
20 Vivanco I, Sawyers CL. The phosphatidylinositol 3-Kinase AKT pathway in human cancer. *Nat Rev Cancer* 2002; **2**: 489–501.
21 Schmitz KJ, Wohlschlaeger J, Lang H *et al.* Activation of the ERK and AKT signalling pathway predicts poor prognosis in hepatocellular carcinoma and ERK activation in cancer tissue is associated with hepatitis C virus infection. *J Hepatol* 2008; **48**: 83–90.
22 Beeram M, Patnaik A, Rowinsky EK. Raf: a strategic target for therapeutic development against cancer. *J Clin Oncol* 2005; **23**: 6771–90.
23 Whittaker S, Marais R, Zhu AX. The role of signaling pathways in the development and treatment of hepatocellular carcinoma. *Oncogene* 2010; **29**: 4989–5005.
24 You WK, McDonald DM. The hepatocyte growth factor/c-Met signaling pathway as a therapeutic target to inhibit angiogenesis. *BMB Rep* 2008; **41**: 833–9.
25 Chan AM, Rubin JS, Bottaro DP *et al.* Identification of a competitive HGF antagonist encoded by an alternative transcript. *Science* 1991; **254**: 1382–5.
26 Yap TA, de Bono JS. Targeting the HGF/c-Met axis: state of play. *Mol Cancer Ther* 2010; **9**: 1077–9.
27 Ke AW, Shi GM, Zhou J *et al.* Role of overexpression of CD151 and/or c-Met in predicting prognosis of hepatocellular carcinoma. *Hepatology* 2009; **49**: 491–503.
28 Kondo S, Ojima H, Tsuda H *et al.* Clinical impact of c-Met expression and its gene amplification in hepatocellular carcinoma. *Int J Clin Oncol* 2013; **18**: 207–13.
29 Lee SJ, Lee J, Sohn I *et al.* A survey of c-MET expression and amplification in 287 patients with hepatocellular carcinoma. *Anticancer Res* 2013; **33**: 5179–86.
30 Cheng AL, Kang YK, Lin D-Y *et al.* Sunitinib versus sorafenib in advanced hepatocellular cancer: results of a randomized phase III trial. *J Clin Oncol* 2013; **31**: 4067–75.

31 Johnson P, Qin S, Park JW *et al.* Brivanib versus sorafenib as first-line therapy in patients with unresectable, advanced hepatocellular carcinoma: results from the randomized phase III BRISK-FL study. *J Clin Oncol* 2013; **31**: 3517–24.
32 Llovet JM, Decaens T, Raoul JL *et al.* Brivanib in patients with advanced hepatocellular carcinoma who were intolerant to sorafenib or for whom sorafenib failed: results from the randomized phase III BRISK-PS study. *J Clin Oncol* 2013; **31**: 3509–16.
33 Cainap C, Qin S, Huang WT *et al.* Phase III trial of linifanib versus sorafenib in patients with advanced hepatocellular carcinoma (HCC). *J Clin Oncol* 2013; **31** (Suppl 4): abstr 249.
34 Zhu AX, Rosmorduc O, Evans J *et al.* SEARCH: a phase III, randomized, double-blind, placebo-controlled trial of sorafenib plus erlotinib in patientswith hepatocellular carcinoma. *Ann Oncol* 2012; **23** (Suppl 9): abstr LBA2.
35 Zhu AX, Kudo M, Assenat E *et al.* Effect of everolimus on survival in advanced hepatocellular carcinoma after failure of sorafenib: the EVOLVE-1 randomized clinical trial. *JAMA* 2014; **312**: 57–67.
36 Zhu AX, Finn RS, Mulcahy M *et al.* A phase II and biomarker study of ramucirumab, a human monoclonal antibody targeting the VEGF receptor-2, as first-line monotherapy in patients with advanced hepatocellular cancer. *Clin Cancer Res* 2013; **19**: 6614–23.
37 Zhu AX, Ryoo B, Yen C *et al.* LBA16 – Ramucirumab (RAM) as second-line treatment in patients (pts) with advanced hepatocellular carcinoma (HCC) following first-line therapy with sorafenib: results from the randomized phase III REACH study. *ESMO Congress* 2014; abstr LBA16.
38 Koyama N, Saito K, Nishioka Y *et al.* Pharmacodynamic change in plasma angiogenic proteins: a dose-escalation phase 1 study of the multi-kinase inhibitor lenvatinib. *BMC Cancer* 2014; **14**: 530.
39 Finn R, Cheng A, Ikeda K *et al.* A multicenter, open-label, phase III trial to compare the efficacy and safty of Lenvatinib versus sorafenib in first-line treatment of patients with unresectable hepatocellular carcinoma. *J Clin Oncol* 2014; **32** (Suppl): abstr TPS4153.
40 Mross K, Frost A, Steinbild S *et al.* A phase I dose-escalation study of regorafenib (BAY 73-4506), an inhibitor of oncogenic, angiogenic, and stromal kinases, in patients with advanced solid tumors. *Clin Cancer Res* 2012; **18**: 2658–67.
41 Bruix J, Tak WY, Gasbarrini A *et al.* Regorafenib as second-line therapy for intermediate or advanced hepatocellular carcinoma: multicentre, open-label, phase II safety study. *Eur J Cancer* 2013; **49**: 3412–9.
42 Adjei AA, Schwartz B, Garmey E. Early clinical development of ARQ 197, a selective, non-ATP-competitive inhibitor targeting MET tyrosine kinase for the treatment of advanced cancers. *Oncologist* 2011; **16**: 788–99.
43 Abou-Alfa GK, Venook AP. The antiangiogenic ceiling in hepatocellular carcinoma: does it exist and has it been reached? *Lancet Oncol* 2013; **14**: e283–8.
44 Cohn AL, Kelley RK, Yang TS *et al.* Activity of cabozantinib (XL184) in hepatocellular carcinoma patients: results from a phase II randomized discontinuation trial (RDT). *J Clin Oncol* 2012; **30** (Suppl): abstr 4007.
45 Verslype C, Cohn A, Kelley R *et al.* Activity of cabozantinib (XL184) in hepatocellular carcinoma: results from a phase II randomized discontinuation trial (RDT). *J Clin Oncol* 2012; **30** (Suppl): abstr 4007.
46 Fernández M, Semela D, Bruix J *et al.* Angiogenesis in liver disease. *J Hepatol* 2009; **50**: 604–20.
47 Kudo M, Imanaka K, Chida N *et al.* Phase III study of sorafenib after transarterial chemoembolisation in Japanese and Korean patients with unresectable hepatocellular carcinoma. *Eur J Cancer* 2011; **47**: 2117–27.
48 Kudo M, Han G, Finn RS *et al.* Brivanib as adjuvant therapy to transarterial chemoembolization in patients with hepatocellular carcinoma: a randomized phase III trial. *Hepatology* 2014; **60**: 1697–707.
49 Kanai F, Yoshida H, Tateishi R *et al.* A phase I/II trial of the oral antiangiogenic agent TSU-68 in patients with advanced hepatocellular carcinoma. *Cancer Chemother Pharmacol* 2011; **67**: 315–24.
50 Arao T, Ueshima K, Matsumoto K *et al.* FGF3/FGF4 amplification and multiple lung metastases in responders to sorafenib in hepatocellular carcinoma. *Hepatology* 2013; **57**: 1407–15.
51 Huang XY, Ke AW, Shi GM *et al.* αB-crystallin complexes with 14-3-3ζ to induce epithelial-mesenchymal transition and resistance to sorafenib in hepatocellular carcinoma. *Hepatology* 2013; **57**: 2235–47.
52 Hagiwara S, Kudo M, Nagai T *et al.* Activation of JNK and high expression level of CD133 predict a poor response to sorafenib in hepatocellular carcinoma. *Br J Cancer* 2012; **106**: 1997–2003.
53 Horwitz E, Stein I, Andreozzi M *et al.* Human and mouse VEGFA-amplified hepatocellular carcinomas are highly sensitive to sorafenib treatment. *Cancer Discov* 2014; **4**: 730–43.
54 Abou-Alfa GK, Schwartz L, Ricci S *et al.* Phase II study of sorafenib in patients with advanced hepatocellular carcinoma. *J Clin Oncol* 2006; **24**: 4293–300.
55 Miyahara K, Nouso K, Tomoda T *et al.* Predicting the treatment effect of sorafenib using serum angiogenesis markers in patients with hepatocellular carcinoma. *J Gastroenterol Hepatol* 2011; **26**: 1604–11.
56 Yau T, Yao TJ, Chan P *et al.* The significance of early alpha-fetoprotein level changes in predicting clinical and survival benefits in advanced hepatocellular carcinoma patients receiving sorafenib. *Oncologist* 2011; **16**: 1270–9.
57 Kuzuya T, Asahina Y, Tsuchiya K *et al.* Early decrease in α-fetoprotein, but not des-γ-carboxy prothrombin, predicts sorafenib efficacy in patients with advanced hepatocellular carcinoma. *Oncology* 2011; **81**: 251–8.
58 Ueshima K, Kudo M, Takita M *et al.* Des-γ-carboxyprothrombin may be a promising biomarker to

determine the therapeutic efficacy of sorafenib for hepatocellular carcinoma. *Dig Dis* 2011; **29**: 321–5.
59 Miyahara K, Nouso K, Morimoto Y *et al.* Evaluation of the effect of sorafenib using serum NX-des-γ-carboxyprothrombin in patients with hepatocellular carcinoma. *Hepatol Res* 2013; **43**: 1064–70.
60 Tsuchiya K, Asahina Y, Matsuda S *et al.* Changes in plasma vascular endothelial growth factor at 8 weeks after sorafenib administration as predictors of survival for advanced hepatocellular carcinoma. *Cancer* 2014; **120**: 229–37.
61 Llovet JM, Hernandez-Gea V. Hepatocellular carcinoma: reasons for phase III failure and novel perspectives on trial design. *Clin Cancer Res* 2014; **20**: 2072–9.
62 Llovet JM, Bruix J. Novel advancements in the management of hepatocellular carcinoma in 2008. *J Hepatol* 2008; **48** (Suppl 1): S20–S37.
63 Chan SL, Mo FK, Wong CS *et al.* A study of circulating interleukin 10 in prognostication of unresectable hepatocellular carcinoma. *Cancer* 2012; **118**: 3984–92.

Abdominal Imaging

Abdom Imaging (2015)
DOI: 10.1007/s00261-015-0352-9

Intratumoral artery on contrast-enhanced computed tomography imaging: differentiating intrahepatic cholangiocarcinoma from poorly differentiated hepatocellular carcinoma

Seiji Tsunematsu,[1] Makoto Chuma,[1,5] Toshiya Kamiyama,[2] Noriyuki Miyamoto,[3] Satoshi Yabusaki,[3] Kanako Hatanaka,[4] Tomoko Mitsuhashi,[4] Hirofumi Kamachi,[2] Hideki Yokoo,[2] Tatsuhiko Kakisaka,[2] Yousuke Tsuruga,[2] Tatsuya Orimo,[2] Kenji Wakayama,[2] Jun Ito,[1] Fumiyuki Sato,[1] Katsumi Terashita,[1] Masato Nakai,[1] Yoko Tsukuda,[1] Takuya Sho,[1] Goki Suda,[1] Kenichi Morikawa,[1] Mitsuteru Natsuizaka,[1] Mitsuru Nakanishi,[1] Koji Ogawa,[1] Akinobu Taketomi,[2] Yoshihiro Matsuno,[4] Naoya Sakamoto[1]

[1]Department of Gastroenterology and Hepatology, Graduate School of Medicine, Hokkaido University, 15 Kita, 7 Nishi, Kita-ku, Sapporo 060-8638, Japan
[2]Department of Gastroenterological Surgery, Graduate School of Medicine, Hokkaido University, Sapporo, Japan
[3]Department of Diagnostic and Interventional Radiology, Graduate School of Medicine, Hokkaido University, Sapporo, Japan
[4]Department of Surgical Pathology, Hokkaido University Hospital, Sapporo, Japan
[5]Gastroenterological Center, Yokohama City University Medical Center, Yokohama, Kanagawa, Japan

Abstract

Aim: Differentiating intrahepatic cholangiocarcinoma (ICC) from poorly differentiated hepatocellular carcinoma (p-HCC) is often difficult, but it is important for providing appropriate treatments. The purpose of this study was to examine the features differentiating ICC from p-HCC on contrast-enhanced dynamic-computed tomography (CT).

Methods: This study examined 42 patients with pathologically confirmed ICC (n = 19) or p-HCC (n = 23) for which contrast-enhanced dynamic CT data were available. CT images were analyzed for enhancement patterns during the arterial phase, washout pattern, delayed enhancement, satellite nodules, capsular retraction, lesion shape, and presence of an intratumoral hepatic artery, intratumoral hepatic vein, intratumoral portal vein, and bile duct dilation around the tumor, portal vein tumor thrombus, lobar atrophy, or lymphadenopathy.

Results: Univariate analysis revealed the presence of rim enhancement (p = 0.037), lobulated shape (p = 0.004), intratumoral artery ($p < 0.001$), and bile duct dilation (p = 0.006) as parameters significantly favoring ICC, while a washout pattern significantly favored p-HCC ($p < 0.001$). Multivariate analysis revealed intratumoral artery as a significant, independent variable predictive of ICC (p = 0.037), and 15 ICCs (78.9%) showed this feature. Washout pattern was a significant, independent variable favoring p-HCC (p = 0.049), with 15 p-HCCs (65.2%) showing this feature.

Conclusion: The presence of an intratumoral artery in the arterial phase on contrast-enhanced dynamic CT was a predictable finding for ICC, and the presence of a washout pattern was a predictable finding for p-HCC, differentiating between ICC and p-HCC.

Key words: Intrahepatic cholangiocarcinoma—Intratumoral artery—Poorly differentiated hepatocellular carcinoma—Contrast-enhanced CT—Differential diagnosis

Correspondence to: Makoto Chuma; *email:* chuma@yokohama-cu.ac.jp

Published online: 13 January 2015

Intrahepatic cholangiocarcinoma (ICC) is the second most common primary liver malignancy after hepatocellular carcinoma (HCC) and originates from the epithelial lining of the intrahepatic bile duct [1]. Several studies have shown that the incidences of ICC and HCC have been increasing [2–4]. Contrast-enhanced dynamic-computed tomography (CT) has a primary role to play in the differential diagnosis of focal liver lesions, including HCC and ICC. Bile duct dilatation and rim-like contrast enhancement are frequently seen on contrast-enhanced CT of ICC [5]. Classic advanced HCC appears as a round tumor showing intense hyperenhancement in the arterial phase, followed by washout during dynamic imaging [6]. Knowledge of the typical imaging features of ICC and HCC would facilitate accurate diagnosis in most cases.

However, advanced HCCs such as poorly differentiated HCC (p-HCC) might not be as hypervascular as classic HCC, which might cause difficulty in differentiation from ICC. Differentiating ICC from p-HCC can reduce the risk of inappropriate treatments for ICC, such as transarterial chemoembolization aimed at HCC. ICC is usually fatal because of the lack of effective non-surgical therapeutic modalities, so correct diagnosis of ICC based on radiological findings may have prognostic significance, particularly in determining treatment methods [7]. Furthermore, definitive diagnosis of ICC will help oncologists to consider adequate treatments, such as complete resection including lymph node dissection.

Although some reports have described the radiological characteristics of ICC and HCC [5, 6, 8, 9], no reports appear to have described imaging findings for pathologically confirmed ICC and p-HCC. On contrast-enhanced CT, intratumoral arteries were often seen in ICC. However, there have been no previous reports that intratumoral arteries on CT distinguish ICC from HCC.

The purpose of this study was to assess the CT features and enhancement patterns differentiating ICC from p-HCC; furthermore, we evaluated whether the presence of an intratumoral artery could be an independent predictor for differentiating ICC from p-HCC.

Methods

Patients

This study was approved by the ethics committees of Hokkaido University Hospital. All study protocols were approved by the institutional review board and performed in compliance with the Declaration of Helsinki.

We retrospectively searched the surgical treatment database at our hospital from July 2003 to December 2012, using the search terms "poorly differentiated HCC" and "ICC." Forty-two patients with histopathological confirmation of either ICC (n = 19) or p-HCC (n = 23) who had undergone contrast-enhanced CT in our institution were included in this study. The final diagnosis of all tumors was confirmed by histopathological examination of surgical specimens. Histological diagnosis was made according to World Health Organization criteria [10, 11]. Combined-type liver cancers were excluded to more clearly investigate differential points of CT imaging between poorly differentiated HCC and ICC. Patient demographics and tumor characteristics are summarized in Table 1.

The 19 patients with ICC included 13 men and 6 women (age range 48–79 years), while the 23 patients with p-HCC included 19 men and 4 women (age range 37–79 years). Serum levels of hepatitis B surface antigen and hepatitis C antibody, alpha-fetoprotein (AFP), protein induced by vitamin K absence or antagonist-II (PIVKA-II), carcinoembryonic antigen (CEA), and carbohydrate antigen 19-9 (CA19-9) were examined preoperatively in all patients.

Image analysis

CT images were obtained by using Aquilion 64 (n = 16, Toshiba Medical Systems, Tochigi, Japan), Aquilion 4-slice CT (n = 12, Toshiba Medical Systems, Tochigi, Japan), light Speed VCT (n = 6, GE, Waukesha, WI, USA), Somatom Volume Zoom (n = 4, Siemens Medical Solutions, Erlangen, Germany), and Somatom Sensation 64 (n = 4, Siemens AG Medical Solutions, Erlangen, Germany).

Unenhanced and 3-phase contrast-enhanced helical CT images were obtained. An automatic bolus-tracking program (Real Prep; Toshiba Medical Systems) was used to time the start of scanning for each phase after contrast material injection. Monitoring was performed at the level of the L1 vertebral body, with the region of interest cursor (0.8–2.0 cm^2) placed in the abdominal aorta. Real-time serial monitoring studies began 10 s after the start of contrast injection. The trigger threshold level was set at 200 Hounsfield units. Arterial phase and portal venous phase scanning started at 20 and 40 s after triggering, respectively. Delayed phase scanning started 180 s after the contrast injection. Contrast material (mean, 450 mg of iodine per kilogram body weight) was delivered over a period of 30 s.

Two radiologists (N.M. and S.Y. with 18 and 8 years of post-training experience in interpreting body CT images, respectively) who had no knowledge of clinical patient information performed all measurements by using a commercially available Digital Imaging and Communications in Medical viewer (VOX BASE; J-MAC, Sapporo, Japan).

The following CT features were evaluated: (1) lesion size; (2) satellite nodules (Fig. 1A); (3) capsular retraction (Fig. 1B); (4) lobulated shape of lesion (Fig. 1C); (5) rim enhancement during arterial phases (Fig. 1C); (6) intrahepatic bile duct dilation around the tumor

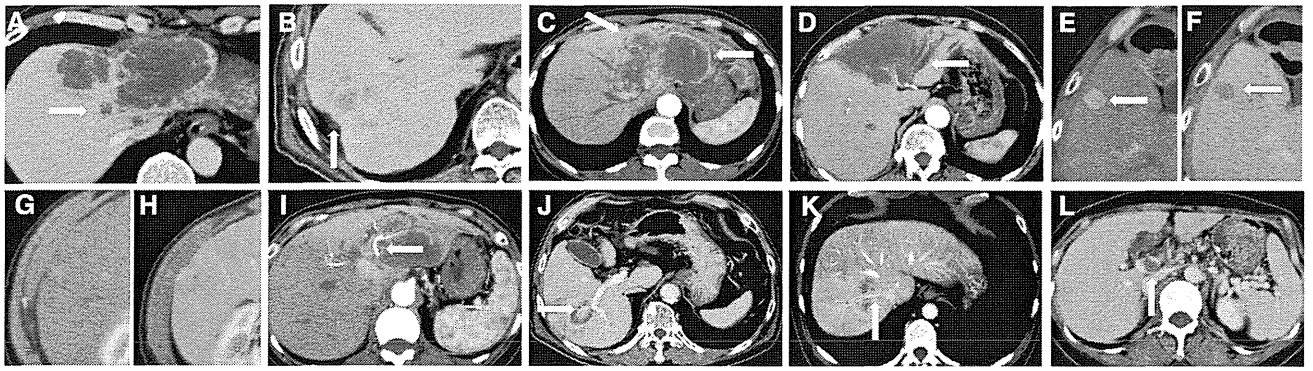

Fig. 1. Evaluated imaging features of contrast-enhanced CT for tumors. **A** CT during the arterial phase with p-HCC shows the satellite nodule (*arrows*). **B** CT during the delayed phase with ICC shows capsular retraction (*arrow*). **C, D** CT during the arterial phase with ICC shows a lobulated lesion and rim enhancement (*arrows*) (**C**) and intrahepatic bile duct dilation around the tumor (*arrow*) (**D**). **E, F** CT during the arterial phase (**E**) and delayed phase (**F**) with p-HCC shows arterial enhancement (**E**) and a washout pattern. **G, H** CT during the arterial phase (**G**) and delayed phase (**H**) with p-HCC shows delayed enhancement. **I–K** CT with ICC shows a hepatic artery running into the tumor (*arrow*) (**I**, arterial phase), a branch of the portal vein running into the tumor (*arrow*) (**J**, portal venous phase), and a hepatic vein running into the tumor (*arrow*) (**K**, delayed phase). **L** CT during the portal venous phase with p-HCC shows tumor thrombus in the portal vein (*arrow*).

Table 1. Patient characteristics of intrahepatic cholangiocarcinoma or poorly differentiated hepatocellular carcinoma

	ICC (n = 19)	p-HCC (*n* = 23)	*p* value
Gender (male/female)	13/6	19/4	0.283
Age (years)	63 (48–79)	62 (37–79)	0.535
Chronic viral hepatitis (HBV/HCV)	3 (2/1)	20 (11/9)	<0.001
Albumin (g/dL)	4.0 (3.1–4.6)	4.0 (3.1–5.2)	0.836
Total bilirubin (mg/dL)	0.8 (0.4–1.4)	0.9 (0.4–2.3)	0.389
Prothrombin time (%)	97 (79.3–135)	87 (66.1–111)	0.038
Platelet ($\times 10^4/\mu L$)	233 (122–354)	135 (42.0–305)	<0.001
AFP (10 ng/mL)	5.8 (2.3–80)	1360 (4.30–39,500)	<0.001
PIVKA-II (40 mAU/mL)	24 (7.0–1400)	208 (9.0–245,600)	0.002
CEA (5 ng/mL)	4.8 (1.0–345)	3.1 (1.4–9.1)	0.287
CA19-9 (37 U/mL)	45.1 (1.0–2590)	47.4 (1.0–237)	0.751

HBV hepatitis B virus, *HCV* hepatitis C virus, *AFP* alpha-fetoprotein, *PIVKA-II* protein induced by vitamin K absence or antagonist-II, *CEA* carcinoembryonic antigen, *CA19-9* cancer-associated carbohydrate antigen 19-9

(Fig. 1D); (7) arterial enhancement (Fig. 1E); (8) washout pattern (Fig. 1E, F); (9) delayed enhancement (Fig. 1G, H); (10) intratumoral artery during arterial phases (Fig. 1I); (11) intratumoral portal vein (Fig. 1J); (12) intratumoral hepatic vein (Fig. 1k) and portal vein tumor thrombus (Fig. 1L); (13) lobar atrophy; and (14) lymphadenopathy. The washout pattern was defined as arterial enhancement (due to the presence of non-triadal neo-angiogenetic arteries) and portal/venous wash out (due to the loss of sinusoidal vascularization) on dynamic imaging.

Particularly, an intratumoral artery was defined as an artery entering the tumor and remaining inside the tumor. Intratumoral portal veins and intratumoral hepatic veins were defined in a similar way. Although minimal discrepancies were seen between readers when interpreting the shape of lesions, consensus decisions for these discrepancies were easily reached during an additional reading session.

Statistical analysis

We statistically analyzed differences in clinical characteristics and CT imaging features between ICC and p-HCC by using the Chi square test for categorical variables and the non-parametric Mann–Whitney *U* test for continuous variables. Significant variables obtained from univariate analysis were applied to multivariate stepwise binary logistic regression analysis to determine the optimal findings for differentiating ICC from p-HCC. Statistical analyses were performed by using the SPSS software package, version 20.0 (IBM, NY). For all tests, values of $p < 0.05$ were considered statistically significant.

Results

Characteristics of patients with ICC or p-HCC

Baseline characteristics of patients with ICC or p-HCC are summarized in Table 1. There were no significant

Table 2. Uni- and multivariate analysis of contrast-enhanced CT features of intrahepatic cholangiocarcinoma and poorly differentiated hepatocellular carcinoma

Pattern	ICC (n = 19)	p-HCC (n = 23)	Univariate analysis p	Multivariate analysis	
				p	Odds ratio (95% CI)
Mean diameter (mm)	64.4 (25–150)	53.7 (10–150)	0.192		
Lobulated shape	14 (73.7)	9 (39.1)	0.004	0.550	1.951 (0.218–17.445)
Satellite nodule	15 (78.9)	14 (60.1)	0.207		
Capsular retraction	6 (31.6)	5 (21.7)	0.407		
Arterial enhancement	9 (47.3)	17 (73.9)	0.078		
Bile duct dilatation	11 (57.9)	4 (17.4)	0.006	0.323	3.445 (0.296–40.070)
Rim enhancement	13 (48.4)	4 (17.4)	0.037	0.158	6.068 (0.495–74.308)
Delayed enhancement	8 (42.1)	7 (30.4)	0.432		
Washout	1 (5.3)	15 (65.2)	<0.001	0.049	0.087 (0.008–0.993)
Intratumoral artery	15 (78.9)	8 (34.8)	<0.001	0.037	10.192 (1.155–89.954)
Intratumoral portal vein	7 (36.8)	2 (8.7)	0.055		
Intratumoral vein	3 (15.8)	2 (8.7)	0.581		
Portal vein tumor thrombus	1 (5.3)	4 (17.4)	0.197		
Lobar atrophy	6 (31.6)	2 (8.7)	0.060		
Lymphadenopathy	4 (21.1)	1 (4.3)	0.094		

Values in parentheses represent percentages

differences between the 2 groups with regard to sex, age, albumin, total bilirubin, CEA, and CA19-9. However, there were differences with respect to chronic viral hepatitis, prothrombin time, platelet counts, AFP, and PIVKA-II.

Analyses of contrast-enhanced CT features of ICC and p-HCC

CT features of ICC and p-HCC and the results of univariate analysis are summarized in Table 2. Lesion diameter ranged from 2.5 to 15.0 cm (mean 64.4 mm) for ICC and from 1.0 to 15.0 cm (mean 53.7 mm) for p-HCC (p = 0.192). Lobulated lesion shape was significantly more rare in patients with p-HCC (n = 9, 39.1%) than in patients with ICC (n = 14, 73.7%) (p = 0.004). The presence of satellite nodules was not statistically significantly different between ICC (n = 15, 78.9%) and p-HCC (n = 14, 60.1%) (p = 0.207). Significant differences in arterial enhancement were not seen between ICC (n = 9, 47.3%) and p-HCC (n = 17, 73.9) (p = 0.078). Capsular retraction was present in patients with ICC (n = 6, 31.6%) or p-HCC (n = 5, 21.7%) (p = 0.407). The presence of intrahepatic bile duct dilation around the tumor differed significantly between the ICC group (n = 11, 57.9%) and the p-HCC group (n = 4, 17.4%) (p = 0.006). Peripheral rim enhancement in the arterial phase was less common in the p-HCC group (n = 4, 17.4%) than in the ICC group (n = 13, 48.4%) (p = 0.037). A washout pattern was more frequent in p-HCC (n = 15, 65.2%) than ICC (n = 1, 5.3%) (p < 0.001). There was no significant difference (p = 0.432) in the occurrence of delayed enhancement in p-HCC (n = 8, 42.1%) and in ICC (n = 7, 30.4%).

An intratumoral artery in the arterial phase was more frequently present for ICC lesions (n = 15, 78.9%) than p-HCC (n = 8, 34.8%) (p < 0.001). The ICC group more frequently showed an intratumoral portal vein (n = 7, 36.8%) than the p-HCC group (n = 2, 8.7%) (p = 0.055). An intratumoral hepatic vein was rarely exhibited in ICCs (n = 3, 15.8%) or p-HCCs (n = 2, 8.7%) (p = 0.581). Portal vein tumor thrombus was also rarely present in ICCs (n = 1, 5.3%) or p-HCCs (n = 4, 17.4%) (p = 0.197).

There was no significant difference (p = 0.060) in the presence of lobar atrophy in ICC (n = 6, 31.6%) and in p-HCC (n = 2, 8.7%). Lymphadenopathy was present in patients with ICC (n = 4, 21.1%) or p-HCC (n = 1, 4.3%) (p = 0.407).

Next, we conducted multivariate binary logistic regression analysis by using significant parameters from the univariate analysis. As shown in Table 2, the presence of an intratumoral artery was an independent CT predictor for differentiating ICC from p-HCC (p = 0.037, odds ratio = 10.192); on the contrary, washout pattern was a significant parameter favoring p-HCC (p = 0.049, odds ratio = 0.087). The presence of an intratumoral artery on CT had a sensitivity of 78.9% and a specificity of 65.2% for ICC. Furthermore, the presence of an intratumoral artery on CT had a positive predictive value of 65.2% and a negative predictive value of 78.9% for ICC.

Case presentation

Representative images from CT and histological features in patients with ICC and p-HCC are shown in Figs. 2 and 3. A 60-year-old man (Case 1) presented with a massive, advanced tumor predominantly located in the right lobe of the liver, and a hepatic artery was seen running into the tumor on CT (Fig. 2A). A right hepatic lobectomy was performed, and histological examination revealed ICC tumor cells that showed infiltrating

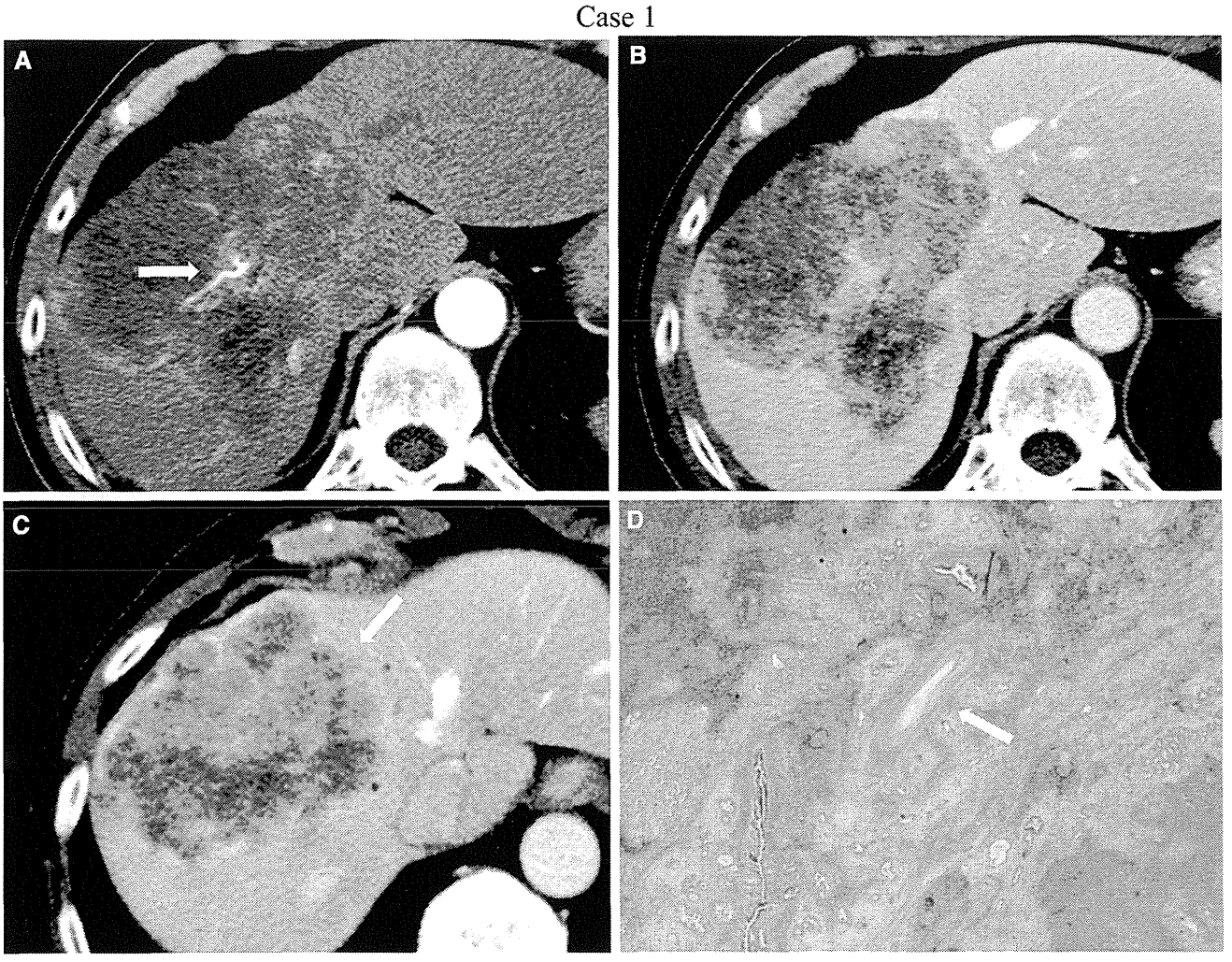

Fig. 2. Contrast-enhanced CT and histological features of ICC. **A** ICC in a 60-year-old man shows a subtle intratumoral artery on arterial phase CT (*arrow*). **B**, **C** CT on delayed phase shows the absence of delayed enhancement (**B**) and the presence of a lobulated shape (**C**). **D** ICC tumor cells show infiltrating replacement growth of the surrounding hepatic parenchyma. An intratumoral artery that has not been destroyed by tumor cells is identified (*arrow*). (Original magnification: d × 10. Hematoxylin and eosin staining).

replacement growth against the surrounding hepatic parenchyma. An intratumoral artery that had not been destroyed by tumor cells was identified (Fig. 2D). A 58-year-old woman (Case 2) presented with a massive, advanced tumor predominantly located in the left lobe of the liver, and no intratumoral artery, portal vein, or hepatic vein was identified on CT (Fig. 3A). A left hepatic lobectomy was performed, and histological examination revealed p-HCC. The tumor was compressing the surrounding liver, and compressed vessels were clearly visible (Fig. 3D).

Discussion

On contrast-enhanced CT, the typical appearance of ICC is a mass that demonstrates thin, rim-like, or thick, band-like contrast enhancement around the tumor during arterial and portal venous phases, with satellite nodules, capsular retraction, lobar atrophy, lymphadenopathy, and delayed enhancement [12–15]. The accuracy of contrast-enhanced CT in diagnosing ICC was 70% [16]. The finding of satellite nodules was associated with tendency to invade small portal vessels and along portal triads. Additionally, scirrhous stroma and biliary involvement of ICC have an influence on the imaging of capsular retraction and lobar atrophy. In our study, a lobulated shape was more closely associated with ICC than with p-HCC on univariate analysis, although satellite nodules, capsular retraction, lobar atrophy, and lymphadenopathy were not different between ICC and p-ICC. The finding of lobulated shape supported the results of previous studies [17, 18]. This trend may be

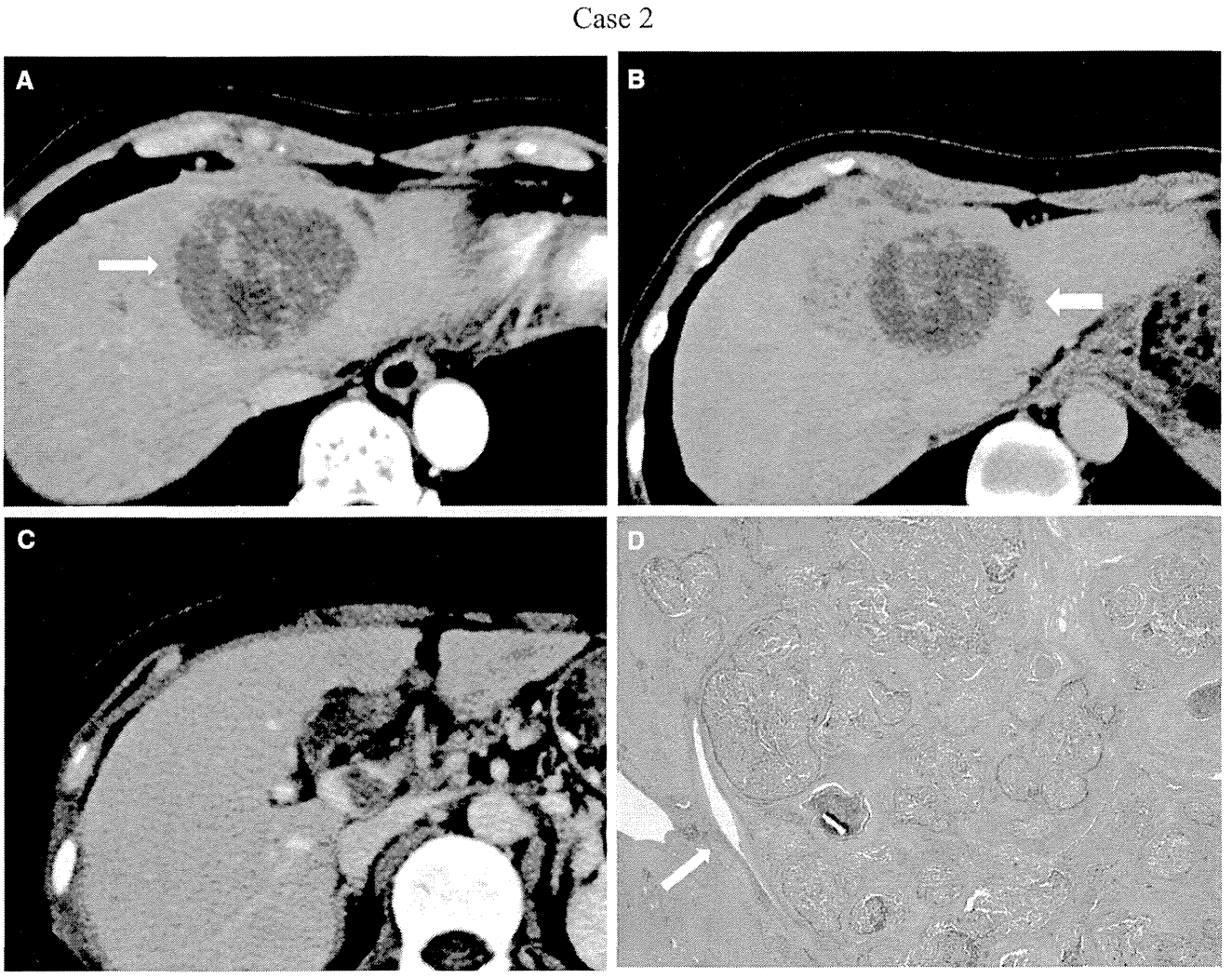

Fig. 3. Contrast-enhanced CT and histological features of p-HCC. **A** p-HCC in a 58-year-old woman shows a low attenuating tumor on arterial phase CT (*arrow*). **B** CT on delayed phase shows nodule (*arrow*) and the absence of delayed enhancement. **C** CT on portal venous phase shows portal vein tumor thrombus. **D** Compressive growth of p-HCC. Tumor compresses the surrounding liver and compressed vessels are clearly visible (*arrow*). (Original magnification: d × 10. Hematoxylin and eosin staining).

related to the fact that ICC tends to invade small portal vein branches adjacent to the main tumor, and the fusion of the primary mass and adjacent satellite tumors results in the lobulated shape [19]. Tumor shape could thus represent a differential feature between ICC and p-HCC.

The frequency of intrahepatic bile duct dilation around the tumor differed between ICC and p-HCC. Eleven of the 19 ICC tumors were accompanied by intrahepatic bile duct dilation around the tumor. The presence of intrahepatic bile duct dilation around the tumor may thus provide a useful clue for differentiation.

In our study, 13 ICC showed rim enhancement during the arterial phase. Rim enhancement patterns differing from p-HCC may relate to different pathological components in the tumor [20]. Fan et al. suggested that the degree of enhancement of ICC depends on the proportion of component fibers and tumor cells, with a tumor rich in cells resulting in strong enhancement [9]. ICC that is peripherally rich in tumor cells with fibrosis in the central portion may result in peripheral rim-like hyperenhancement.

In addition, significant differences in washout patterns were seen between ICC and p-HCC, although there were no significant differences in arterial enhancement and delayed enhancement between the two groups. According to the guidelines of the American Association for the Study of Liver Disease, nodules larger than 1 cm detected in liver cirrhosis may be confidently diagnosed as HCC only when a washout pattern is detected on contrast-enhanced CT or magnetic resonance imaging

[21]. According to our findings, the washout pattern can be useful for identifying p-HCC or ICC. However, distinguishing p-HCC from some ICCs showing diffuse hyperenhancement in the arterial phase and subsequent washout is difficult.

In our present study, 15 (78.9%) of the 19 ICCs showed an intratumoral artery in the arterial phase. Although we occasionally recognized vessels running into the tumor, to the best of our knowledge, no previous reports have described the presence of intratumoral arteries in ICC and p-HCC. In our study, ICCs were able to be differentiated from p-HCCs based on the finding of an intratumoral artery ($p = 0.037$), according to multivariate binary logistic regression analysis. Based on our results, the presence of an intratumoral artery in the arterial phase on contrast-enhanced CT could be a predictive finding for reliable differentiation of ICC from p-HCC. Few reports have described intratumoral arteries of ICC being demonstrated on contrast-enhanced CT. One study showed intratumoral arteries of the ICC identified immediately after the injection of contrast material for CT during hepatic arteriography [22]. Furthermore, that study indicated that tumor enhancement gradually spreads from each intratumoral artery [22]. Infiltrating replacement is an inherent growth feature of ICC, with the surrounding liver gradually incorporated into the tumor as it grows [23]. In this process, the blood vessel is not destroyed by tumor cells and is retained inside. By contrast, HCC shows fibrous encapsulation or compressive growth [24]. With such growth, blood vessels are pressed to the outside of the tumor. Our cases also showed these features (Fig. 2). Such differences in growth type may be related to differences in intratumoral arteries between ICC and HCC. No significant difference was seen between ICC and p-HCC in regard to intratumoral portal veins, intratumoral hepatic veins, or portal vein tumor thrombus. We supposed that intratumoral artery was retained within the ICC rather than portal or hepatic veins because of the stiffness of the arterial wall.

The results of this study have revealed features that allow ICC and p-HCC to be distinguished based on findings from contrast-enhanced CT. In clinical practice, contrast-enhanced CT is a useful diagnostic method to distinguish ICC from p-HCC, since results of tumor marker levels and tissue biopsy are difficult and often indeterminate. The optimal treatment for ICC is complete tumor resection, including lymph node removal [25–27]. In cases of HCC, the treatment modality of choice depending on the degree of cirrhosis is complete resection, topical therapy including radiofrequency ablation or liver transplantation. If the patient has advanced cirrhosis or advanced HCC, then treatments such as transarterial chemoembolization hepatic arterial infusion chemotherapy and systemic chemotherapy are applicable [28, 29]. Because misdiagnosis of ICC as HCC can lead to inadequate medical care, our identification of characteristic findings for ICC may have important practical value in attaining a correct diagnosis.

This study has several limitations that must be considered when interpreting the results. First, our study might have included some degree of selection bias, as we retrospectively analyzed only those patients with ICC or p-HCC who underwent contrast-enhanced CT and hepatic surgery. The absence of the well- and moderately differentiated subtypes of HCC in this study is an important limitation in interpreting our results. Additionally, the numbers of ICCs and p-HCCs were relatively small, because the patient group was limited to those with a pathologic diagnosis determined by surgery. Finally, most tumors were relatively large, and the findings in our results may not be observed in smaller sized tumors.

In conclusion, the presence of an intratumoral artery during arterial phase on enhanced CT is valuable in differentiating between ICC and p-HCC, as is the washout pattern. This new finding may facilitate correct diagnosis and more timely selection of appropriate treatment strategies.

Acknowledgments. This study was supported by Grants from the Ministry of Education, Culture, Sports, Science and Technology-Japan; Ministry of Health, Labour and Welfare-Japan; and Japan Health Sciences Foundation.

Conflict of interest. The authors declare that they have no conflicts of interest.

References

1. Kham SA, Thomas HC, Davidson BR, et al. (2005) Cholangiocarcinoma. Lancet 366:1303–1314
2. Patel T (2001) Increasing incidence and mortality of primary intrahepatic cholangiocarcinoma in the United States. Hepatology 33:1353–1357
3. Singh P, Patel T (2006) Advances in the diagnosis, evaluation and management of cholangiocarcinoma. Curr Opin Gastroenterol 22:294–299
4. Shaib Y, El-Serag HB (2004) The epidemiology of cholangiocarcinoma. Semin Liver Dis 24:115–125
5. Valls C, Guma A, Puig I, et al. (2000) Intrahepatic peripheral cholangiocarcinoma: CT evaluation. Abdom Imaging 25:490–496
6. Bruix J, Sherman M (2005) Practice Guidelines Committee, American Association for the Study of Liver Diseases. Management of hepatocellular carcinoma. Hepatology 42:1208–1236
7. Khan SA, Davidson BR, Goldin R, et al. (2002) Guidelines for the diagnosis and management of cholangiocarcinoma. Gut 61:1657–1669
8. Choi BI, Han JK, Shin YM, et al. (1995) Peripheral cholangiocarcinoma: comparison of MRI with CT. Abdom Imaging 20:357–360
9. Fan ZM, Yamashita Y, Harada M, et al. (1993) Intrahepatic cholangiocarcinoma: spin-echo and contrast-enhanced dynamic MR imaging. Am J Roentgenol 161:313–317
10. Hirohashi S, Ishak KG, Kojiro M, et al. (2000) Hepatocellular carcinoma. In: Hamilton SRAL (ed) *World Health Organization classification of tumours pathology and genetics of tumours of the digestive system.* Lyon: IARC Press, pp 159–172
11. Nakanuma Y, Leong AS-Y, Sripa B, et al. (2000) Intrahepatic cholangiocarcinoma. In: Hamilton SR (ed) *World Health Organization classification of tumours Pathology and genetics of tumours of the digestive system.* Aaltonen: IARC Press, pp 173–180

12. Lee WJ, Lim HK, Jang KM, et al. (2001) Radiologic spectrum of cholangiocarcinoma: emphasis on unusual manifestations and differential diagnosis. Radiographics 21:97–116
13. Han JK, Choi BI, Kim AY, et al. (2002) Cholangiocarcinoma: pictorial essay of CT and cholangiographic findings. Radiographics 22:173–187
14. Baheti AD, Tirumani SH, Rosenthal MH, Shinagare AB, Ramaiya NH (2014) Diagnosis and management of intrahepatic cholangiocarcinoma: a comprehensive update for the radiologist. Clin Radiol 69:e463–e470
15. Kim TK, Choi BI, Han JK, et al. (1997) Peripheral cholangiocarcinoma of the liver: two-phase helical CT findings. Radiology 204:539–543
16. Olnes MJ, Erlich R (2004) A review and update on cholangiocarcinoma. Oncology 66:167–179
17. Choi BI, Han JK, Shin YM, et al. (1995) Peripheral cholangiocarcinoma: comparison of MRI with CT. Abdom Imaging 20:357–360
18. Valls C, Guma A, Puig I, et al. (2000) Intrahepatic peripheral cholangiocarcinoma: CT evaluation. Abdom Imaging 25:490–496
19. Lim JH (2003) Cholangiocarcinoma: morphologic classification according to growth pattern and imaging findings. Am J Roentgenol 181:819–827
20. Ros PR, Buck JL, Goodman ZD, et al. (1988) Intrahepatic cholangiocarcinoma: radiologic-pathologic correlation. Radiology 167:689–693
21. Bruix J, Sherman M (2011) American association for the study of liver diseases. Management of hepatocellular carcinoma: an update. Hepatology 53:1020–1022
22. Miura F, Okazumi S, Takayama W, et al. (2004) Hemodynamics of intrahepatic cholangiocarcinoma: evaluation with single-level dynamic CT during hepatic arteriography. Abdom Imaging 29:467–471
23. Kozaka K, Sasaki M, Fujii T, et al. (2007) A subgroup of intrahepatic cholangiocarcinoma with an infiltrating replacement growth pattern and a resemblance to reactive proliferating bile ductules: bile ductular carcinoma. Histopathology 51:390–400
24. Ueda K, Terada T, Nakanuma Y, et al. (1992) Vascular supply in adenomatous hyperplasia of the liver and hepatocellular carcinoma: a morphometric study. Hum. Pathol 23:619–626
25. Singh P, Patel T (2006) Advances in the diagnosis, evaluation and management of cholangiocarcinoma. Curr Opin Gastroenterol 22:294–299
26. Jarnagin WR, Shoup M (2004) Surgical management of cholangiocarcinoma. Semin Liver Dis 24:189–199
27. Nagorney DM, Donohue JH, Farnell MB, et al. (1993) Outcomes after curative resections of cholangiocarcinoma. Arch Surg 128:871–879
28. Bruix J, Sherman M, Llovet JM, et al. (2001) Clinical management of hepatocellular carcinoma: conclusions of the Barcelona-2000 EASL conference. J Hepatol 35:421–430
29. Hertl M, Cosimi AB (2005) Liver transplantation for malignancy. Oncologist 10:269–281

THE JOURNAL OF BIOLOGICAL CHEMISTRY VOL. 290, NO. ??, pp. 1-xxx, ???? ??, 2015

Dysregulation of Retinoic Acid Receptor Diminishes Hepatocyte Permissiveness to Hepatitis B Virus Infection through Modulation of Sodium Taurocholate Cotransporting Polypeptide (NTCP) Expression*

Received for publication, August 4, 2014, and in revised form, December 20, 2014 Published, JBC Papers in Press, December 30, 2014, DOI 10.1074/jbc.M114.602540

Senko Tsukuda[‡§], Koichi Watashi[‡1], Masashi Iwamoto[‡], Ryosuke Suzuki[‡], Hideki Aizaki[‡], Maiko Okada[¶], Masaya Sugiyama[‖], Soichi Kojima[§], Yasuhito Tanaka[**], Masashi Mizokami[‖], Jisu Li[‡‡], Shuping Tong[‡‡], and Takaji Wakita[‡]

From the [‡]Department of Virology II, National Institute of Infectious Diseases, Tokyo 162-8640, Japan, the [§]Micro-signaling Regulation Technology Unit, RIKEN Center for Life Science Technologies, Wako 351-0198, Japan, the [¶]Department of Translational Oncology, St. Marianna University School of Medicine, Kawasaki 216-8511, Japan, the [‖]Research Center for Hepatitis and Immunology, National Center for Global Health and Medicine, Ichikawa 272-8516, Japan, the [**]Department of Virology and Liver Unit, Nagoya City University Graduate School of Medicinal Sciences, Nagoya 467-8601, Japan, and the [‡‡]Liver Research Center Rhode Island Hospital, Warren Alpert School of Medicine, Brown University, Providence, Rhode Island 02912

Background: Host factors regulating hepatitis B virus (HBV) entry receptors are not well defined.
Results: Chemical screening identified that retinoic acid receptor (RAR) regulates sodium taurocholate cotransporting polypeptide (NTCP) expression and supports HBV infection.
Conclusion: RAR regulates NTCP expression and thereby supports HBV infection.
Significance: RAR regulation of NTCP can be a target for preventing HBV infection.

Sodium taurocholate cotransporting polypeptide (NTCP) is an entry receptor for hepatitis B virus (HBV) and is regarded as one of the determinants that confer HBV permissiveness to host cells. However, how host factors regulate the ability of NTCP to support HBV infection is largely unknown. We aimed to identify the host signaling that regulated NTCP expression and thereby permissiveness to HBV. Here, a cell-based chemical screening method identified that Ro41-5253 decreased host susceptibility to HBV infection. Pretreatment with Ro41-5253 inhibited the viral entry process without affecting HBV replication. Intriguingly, Ro41-5253 reduced expression of both NTCP mRNA and protein. We found that retinoic acid receptor (RAR) regulated the promoter activity of the human *NTCP* (h*NTCP*) gene and that Ro41-5253 repressed the hNTCP promoter by antagonizing RAR. RAR recruited to the h*NTCP* promoter region, and nucleotides −112 to −96 of the h*NTCP* was suggested to be critical for RAR-mediated transcriptional activation. HBV susceptibility was decreased in pharmacologically RAR-inactivated cells. CD2665 showed a stronger anti-HBV potential and disrupted the spread of HBV infection that was achieved by continuous reproduction of the whole HBV life cycle. In addition, this mechanism was significant for drug development, as antagonization of RAR blocked infection of multiple HBV genotypes and also a clinically relevant HBV mutant that was resistant to nucleoside analogs. Thus, RAR is crucial for regulating NTCP expression that determines permissiveness to HBV infection. This is the first demonstration showing host regulation of NTCP to support HBV infection.

Hepatitis B virus (HBV)[2] infection is a major public health problem, as the virus chronically infects ~240 million people worldwide (1–3). Chronic HBV infection elevates the risk for developing liver cirrhosis and hepatocellular carcinoma (4–6). Currently, two classes of antiviral agents are available to combat chronic HBV infection. First, interferon (IFN)-based drugs, including IFNα and pegylated-IFNα, modulate host immune function and/or directly inhibit HBV replication in hepatocytes (7, 8). However, the antiviral efficacy of IFN-based drugs is restricted to less than 40% (9, 10). Second, nucleos(t)ide analogs, including lamivudine (LMV), adefovir, entecavir (ETV), tenofovir, and telbivudine suppress HBV by inhibiting the viral reverse transcriptase (11, 12). Although they can provide significant clinical improvement, long term therapy with nucleos(t)ide analogs often results in the selection of drug-resistant mutations in the target gene, which limits the treatment outcome. For example, in patients treated with ETV, at least three mutations can arise in the reverse transcriptase sequence of the

* This work was supported in part by grants-in-aid from the Ministry of Health, Labor, and Welfare, Japan, from the Ministry of Education, Culture, Sports, Science, and Technology, Japan, and from Japan Society for the Promotion of Science, and by the incentive support from Liver Forum in Kyoto.

[1] To whom correspondence should be addressed: Dept. of Virology II, National Institute of Infectious Diseases, 1-23-1 Toyama, Shinjuku-ku, Tokyo, 162-8640, Japan. Tel.: 81-3-5285-1111; Fax: 81-3-5285-1161; E-mail: kwatashi@nih.go.jp.

[2] The abbreviations used are: HBV, hepatitis B virus; NTCP, sodium taurocholate cotransporting polypeptide; RAR, retinoic acid receptor; LMV, lamivudine; ETV, entecavir; HB, HBV surface protein; SLC10A1, solute carrier protein 10A1; hNTCP, human NTCP; ATRA, all-*trans*-retinoic acid; SHP, small heterodimer partner; ASBT, apical sodium-dependent bile salt transporter; RARE, RAR-responsive element; RXR, retinoid X receptor; SEAP, secreted alkaline phosphatase; FXR, farnesoid X receptor; MTT, 3-(4,5-dimethylthiazol-2-yl)-2,5-diphenyltetrazolium bromide; nt, nucleotide; cccDNA, covalently closed circular DNA.

polymerase L180M and M204V plus either one of Thr-184, Ser-202, or Met-250 codon changes to acquire drug resistance (13). Therefore, development of new anti-HBV agents targeting other molecules requires elucidation of the molecular mechanisms underlying the HBV life cycle.

HBV infection of hepatocytes involves multiple steps. The initial viral attachment to the host cell surface starts with a low affinity binding involving heparan sulfate proteoglycans, and the following viral entry is mediated by a specific interaction between HBV and its host receptor(s) (14). Recently, sodium taurocholate cotransporting polypeptide (NTCP) was reported as a functional receptor for HBV (15). NTCP interacts with HBV large surface protein (HBs) to mediate viral attachment and the subsequent entry step. NTCP, also known as solute carrier protein 10A1 (SLC10A1), is physiologically a sodium-dependent transporter for bile salts located on the basolateral membrane of hepatocytes (16). In the liver, hepatocytes take up bile salts from the portal blood and secrete them into bile for enterohepatic circulation, and NTCP-mediated uptake of bile salts into hepatocytes occurs largely in a sodium-dependent manner. Although NTCP is abundant in freshly isolated primary hepatocytes, it is weakly or no longer expressed in most cell lines such as HepG2 and Huh-7, and these cells rarely support HBV infection (17, 18). In contrast, primary human hepatocytes, primary tupaia hepatocyte, and differentiated HepaRG cells, which are susceptible to HBV infection, express significant levels of NTCP (19). Thus, elucidation of the regulatory mechanisms for *NTCP* gene expression is important for understanding the HBV susceptibility of host cells as well as for developing a new anti-HBV strategy. HBV entry inhibitors are expected to be useful for preventing *de novo* infection after liver transplantation, for post-exposure prophylaxis, or for vertical transmission by short term treatment (20, 21).

In this study, we used a HepaRG-based HBV infection system to screen for small molecules capable of decreasing HBV infection. We found that pretreatment of host cells with Ro41-5253 reduced HBV infection. Ro41-5253 reduced NTCP expression by repressing the promoter activity of the human *NTCP* (h*NTCP*) gene. Retinoic acid receptor (RAR) played a crucial role in regulating the promoter activity of h*NTCP*, and Ro41-5253 antagonized RAR to reduce *NTCP* transcription and consequently HBV infection. This and other RAR inhibitors showed anti-HBV activity against different genotypes and an HBV nucleoside analog-resistant mutant and moreover inhibited the spread of HBV. This study clarified one of the mechanisms for gene regulation of NTCP to support HBV permissiveness, and it also suggests a novel concept whereby manipulation of this regulation machinery can be useful for preventing HBV infection.

EXPERIMENTAL PROCEDURES

Reagents—Heparin was obtained from Mochida Pharmaceutical. Lamivudine, cyclosporin A, all-*trans*-retinoic acid (ATRA), and TO901317 were obtained from Sigma. Entecavir was obtained from Santa Cruz Biotechnology. Ro41-5253 was obtained from Enzo Life Sciences. PreS1-lipopeptide and FITC-labeled preS1 were synthesized by CS Bio. IL-1β was purchased from PeproTech. CD2665, BMS195614, BMS493, and MM11253 were purchased from Tocris Bioscience.

Cell Culture—HepaRG cells (BIOPREDIC) and primary human hepatocytes (Phoenixbio) were cultured as described previously (19). HepG2 and HepAD38 cells (kindly provided by Dr. Christoph Seeger at Fox Chase Cancer Center) (22) were cultured with DMEM/F-12 + GlutaMAX (Invitrogen) supplemented with 10 mM HEPES (Invitrogen), 200 units/ml penicillin, 200 μg/ml streptomycin, 10% FBS, and 5 μg/ml insulin. HuS-E/2 cells (kindly provided by Dr. Kunitada Shimotohno at National Center for Global Health and Medicine) were cultured as described previously (23).

Plasmid Construction—phNTCP-Gluc, pTK-Rluc was purchased from GeneCopoeia and Promega, respectively. pRARE-Fluc was generated as described (25). For constructing phNTCP-Gluc carrying a mutation in a putative RARE (nt −491 to −479), the DNA fragments were amplified by PCR using phNTCP-Gluc as a template with the following primer sets: F1, 5′-CAGATCTTGGAATTCCCAAAATC-3′ and 5′-GAGGGGATGTGTCCATTGAAATGTTAATGGGAGCT-GAGAGGATGCCAGTATCCTCCCT-3′ and primer sets 5′-CTCTCAGCTCCCATTAACATTTCAATGGACACATCC-CCTCCTGGAGGCCAGTGACATT-3′ and R6, 5′-CTCGGT-ACCAAGCTTTCCTTGTT-3′. The resultant products were further amplified by PCR with F1 and R6 and then inserted into the EcoRI/HindIII sites of phNTCP-Gluc to generate phNTCP Mut(−491 to −479)-Gluc. Other promoter mutants were prepared by the same method using the following primer sets: F1, 5′-GTGGGTTATCATTTGTTTCCCGAAAACATTAG-AGTGAAAGGAGCTGGGTGTTGCCTTTGG-3′ and 5′-TCCTTTCACTCTAATGTTTTCGGGAAACAAATGATA-ACCCACTGGACATGGGGAGGGCAC-3′; R6 for −368 to −356; F1 and 5′-AATCTAGGTCCAGCCTATTTAAGTCC-CTAAATTTCCTTTTCCCAGCTCCGCTCTTGATTCCTT-3′, 5′-CTGGGAAAAGGAAATTTAGGGACTTAAATAGG-CTGGACCTAGATTCAGGTGGGCCCTGGGCAG-3′, and R6 for −274 to −258; F1 and 5′-TTCTGGGCTTATTTCTA-TATTTTGCAATCCACTGAGTGTGCCTCATGGGCATT-CATTC-3′, 5′-CACACTCAGTGGATTGCAAAATATAGA-AATAAGCCCAGAAGCAGCAAAGTGACAAGGG-3′, and R6 for −179 to −167; F1 and 5′-AGCTCTCCCAAGCTCAA-AGATAAATGCTAGTTTCCTGGGTGCTACTTGTACTC-CTCCCTTGTC-3′, 5′-GTAGCACCCAGGAAACTAGCAT-TTATCTTTGAGCTTGGGAGAGCTAGGGCAGGCAGAT-AAGGT-3′, and R6 for −112 to −96, respectively. For constructing the hNTCP promoter carrying these five mutations (5-Mut), five DNA segments were amplified using the primers as follows: segment 1, F1 and 5′-GAGGGGATGTGTCCATG-ACC-3′; segment 2, 5′-AGCTCCTTTCACTCTCATGGGT-3′ and 5′-TCCTTTTCCCAGCTCCGC-3′; segment 3, 5′-GAG-CTGGGAAAAGGAGCTGC-3′ and 5′-CCACTGAGTGTG-CCTCATGG-3′; segment 4, 5′-AGGCACACTCAGTGGA-GGG-3′ and 5′-CTGGGTGCTACTTGTACTCCTCC-3′; and segment 5, 5′-CAAGTAGCACCCAGGAATCCA-3′ and R6. For producing a deletion construct for the h*NTCP* promoter, phNTCP (−53 to +108)-Gluc, DNA fragment was amplified using the primer sets 5′-GGTGAATTCTGTTCCTCTTTGG-GGCGACAGC-3′ and 5′-GGTGGTAAGCTTTCCTTGTTC-

TCCGGCTGACTCC-3′ and then inserted into the EcoRI and HindIII sites of phNTCP-Gluc.

HBV Preparation and Infection—HBV was prepared and infected as described (19). HBV used in this study was mainly derived from HepAD38 cells (22). For Fig. 8, *A–E,* we used concentrated (~200-fold) media of HepG2 cells transfected with an expression plasmid for either HBV genotypes A, B, C, D or genotype C carrying mutations at L180M, S202G, and M204V (HBV/Aeus, HBV/Bj35s, HBV/C-AT, HBV/D-IND60, or HBV/C-AT(L180M/S202G/M204V)) (24) and infected into the cells at 2000 GEq/cell in the presence of 4% PEG8000 at 37 °C for 16 h as described previously (19). HBV for Fig. 8*F* (genotype C) was purchased from Phoenixbio.

Real Time PCR and RT-PCR—Real time PCR for detecting HBV DNAs and cccDNA was performed as described (19). RT-PCR detection of mRNAs for *NTCP, ASBT, SHP,* and *GAPDH* was performed with one-step RNA PCR kit (TaKaRa) following the manufacturer's protocol with primer set 5′-AGGGAGGAGGTGGCAATCAAGAGTGG-3′ and 5′-CCGGCTGAAGAACATTGAGGCACTGG-3′ for *NTCP,* 5′-GTTGGCCTTGGTGATGTTCT-3′ and 5′-CGACCCAATAGGCCAAGATA-3′ for *ASBT,* 5′-CAGCTATGTGCACCTCATCG-3′ and 5′-CCAGAAGGACTCCAGACAGC-3′ for *SHP,* and 5′-CCATGGAGAAGGCTGGGG-3′ and 5′-CAAAGTTGTCATGGATGACC-3′ for *GAPDH,* respectively.

Immunofluorescence Analysis—Immunofluorescence was conducted essentially as described (25) using an anti-HBc antibody (DAKO, catalog no. B0586) at a dilution of 1:1000.

Detection of HBs and HBe Antigens—HBs and HBe antigens were detected by ELISA and chemiluminescence immunoassay, respectively, as described (19).

MTT Assay—The MTT cell viability assay was performed as described previously (19).

Southern Blot Analysis—Isolation of cellular DNA and Southern blot analysis to detect HBV DNAs were performed as described previously (19).

Immunoblot Analysis—Immunoblot analysis was performed as described previously (26, 27). Anti-NTCP (Abcam) (1:2000 dilution), anti-RARα (Santa Cruz Biotechnology) (1:6000 dilution), anti-RARβ (Sigma) (1:6000 dilution), anti-RARγ (Abcam) (1:2000 dilution), anti-RXRα (Santa Cruz Biotechnology) (1:8000 dilution), and anti-actin (Sigma) (1:5000 dilution) antibodies were used for primary antibodies.

Flow Cytometry—1×10^6 primary human hepatocytes were incubated for 30 min with a 1:50 dilution of anti-NTCP antibody (Abcam) and then washed and incubated with a dye-labeled secondary antibody (Alexa Fluor 488, Invitrogen) at 1:500 dilution in the dark. Staining and washing were carried out at 4 °C in PBS supplemented with 0.5% bovine serum albumin and 0.1% sodium azide. The signals were analyzed with Cell Sorter SH8000 (Sony).

FITC-preS1 Peptide-binding Assay—Attachment of preS1 peptide with host cells was examined by preS1 binding assay essentially as described previously (28). HepaRG cells treated with or without Ro41-5253 (28) for 24 h or unlabeled preS1 peptide for 30 min were incubated with 40 nM FITC-labeled preS1 peptide (FITC-preS1) at 37 °C for 30 min. After washing the cells twice with culture medium and once with phosphate-buffered saline (PBS), the cells were fixed with 4% paraformaldehyde. Then the cells were treated with 4% Block Ace (DS Pharma Biomedical) containing DAPI for 30 min.

Reporter Assay—HuS-E/2 cells were transfected with phNTCP-Gluc (GeneCopoeia), a reporter plasmid carrying the *NTCP* promoter sequence upstream of the Gaussia luciferase (Gluc) gene, and pSEAP (GeneCopoeia), expressing the secreted alkaline phosphatase (SEAP) gene, together with or without expression plasmids for RARα, RARβ, RARγ, with RXRα using Lipofectamine 2000 (Invitrogen). At 24 h post-transfection, cells were stimulated with the indicated compounds for a further 24 h. The activities for Gluc as well as for SEAP were measured using a Secrete-Pair Dual-Luminescence assay kit (GeneCopoeia) according to the manufacturer's protocol, and Gluc values normalized by SEAP are shown.

pRARE-Fluc, carrying three tandem repeats of RAR-binding elements upstream of firefly luciferase (Fluc), and pTK-Rluc (Promega), which carries herpes simplex virus thymidine kinase promoter expressing *Renilla* luciferase (Rluc) (25), were used in dual-luciferase assays for detecting Fluc and Rluc. Fluc and Rluc were measured with Dual-Luciferase Reporter Assay System (Promega) according to the manufacturer's protocol, and Fluc activities normalized by Rluc are shown.

For evaluating HBV transcription in Fig. 2*B,* we used a reporter construct carrying HBV enhancer I, II, and core promoter (nt 1039–1788) ("Enh I + II") and that carrying enhancer II and core promoter (nt 1413–1788) ("Enh II"). These were constructed by inserting the corresponding sequences derived from a genotype D HBV in HepG2.2.15 cells into pGL4.28 vector (Promega). pGL3 promoter vector (Promega), which carries SV40 promoter ("SV40") was used as a control.

Chromatin Immunoprecipitation (ChIP) Assay—ChIP assay was performed using a Pierce-agarose ChIP kit (Thermo Fisher Scientific) according to the manufacturer's instructions. Huh7-25 cells transfected with phNTCP-Gluc together with or without expression plasmids for FLAG-tagged RARa and for RXRa were treated with 5 mg/ml actinomycin D for 2 h. The cells were then washed and treated with or without 2 mM ATRA for 60 min. Formaldehyde cross-linked cells were lysed, digested with micrococcal nuclease, and immunoprecipitated with anti-FLAG antibody (Sigma) or normal IgG. Input samples were also recovered without immunoprecipitation. DNA recovered from the immunoprecipitated or the input samples was amplified with primers 5′-CCCAGGGCCCACCTGAATCTA-3′ and 5′-TAGATTCAGGTGGGCCCTGGG-3′ for detection of NTCP.

RESULTS

Anti-HBV Activity of Ro41-5253—We searched for small molecules capable of decreasing HBV infection in a cell-based chemical screening method using HBV-susceptible HepaRG cells (29). As a chemical library, we used a set of compounds for which bioactivity was already characterized (19). HepaRG cells were pretreated with compounds and then further incubated with HBV inoculum in the presence of compounds for 16 h (Fig. 1*A*). After removing free HBV and compounds by washing, the cells were cultured for an additional 12 days without compounds. For robust screening, HBV infection was monitored by F1

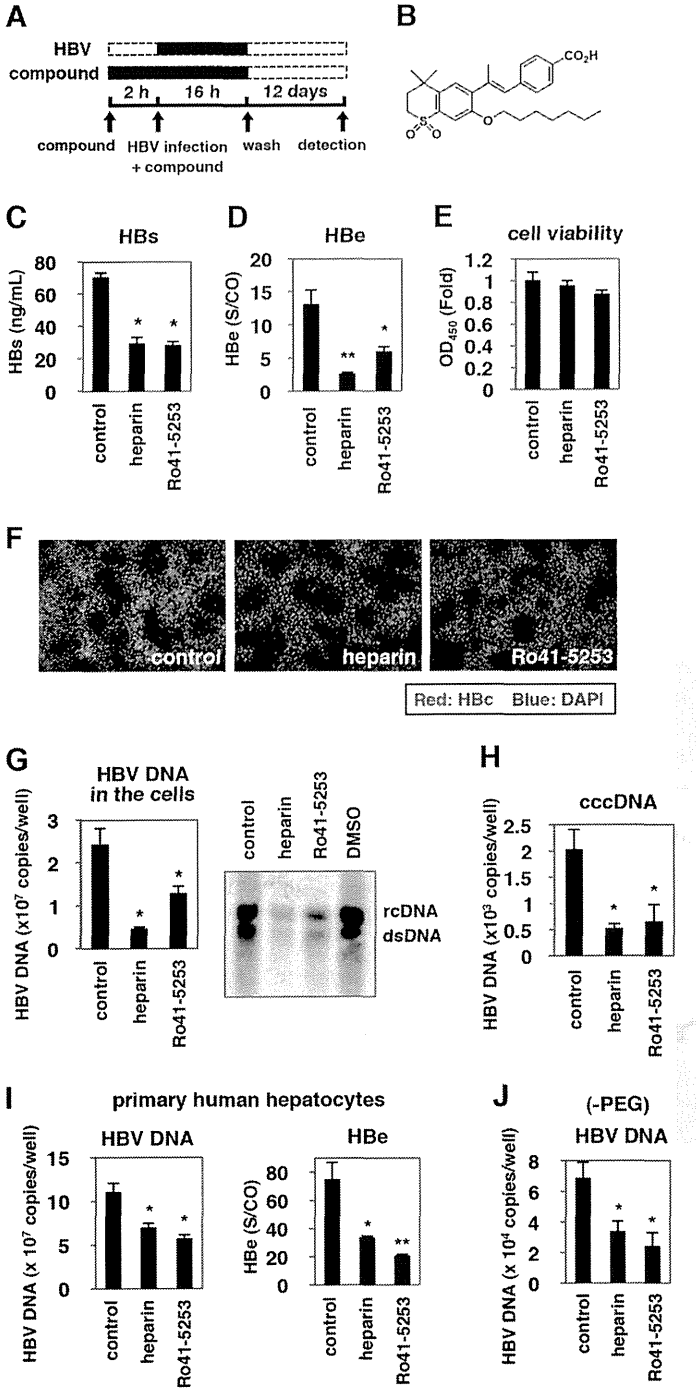

FIGURE 1. **Ro41-5253 decreased susceptibility to HBV infection.** *A*, schematic representation of the schedule for treatment of HepaRG cells with compounds and infection with HBV. HepaRG cells were pretreated with compounds for 2 h and then inoculated with HBV in the presence of compounds for 16 h. After washing out the free HBV and compounds, cells were cultured in the absence of compounds for an additional 12 days followed by quantification of secreted HBs protein. *Black* and *dashed bars* indicate the interval for treatment and without treatment, respectively. *B*, chemical structure of Ro41-5253. *C–E*, HepaRG cells were treated with or without 10 μM Ro41-5253 or 50 units/ml heparin according to the protocol shown in *A*, and HBs (*C*) and HBe (*D*) antigens in the culture supernatant were measured. Cell viability was also examined by MTT assay (*E*). *F–H*, HBc protein (*F*), HBV DNAs (*G*), and cccDNA (*H*) in the cells according to the protocol shown in *A* were detected by immunofluorescence, real time PCR, and Southern blot analysis. *Red* and *blue* in *F* show the detection of HBc protein and nuclear staining, respectively. *I* and *J*, primary human hepatocytes were treated with the indicated compounds and infected with HBV in the presence (*I*) or absence (*J*) of PEG8000 according to the protocol shown in *A*. The levels of HBV DNA in the cells (*I* and *J*) and HBe antigen in the culture supernatant (*I*) were quantified. The data show the means of three independent experiments. Standard deviations are also shown as *error bars*. Statistical significance was determined using Student's *t* test (*, $p < 0.05$; **, $p < 0.01$).

ELISA quantification of HBs antigen secreted from the infected cells at 12 days postinfection. This screening revealed that HBs was significantly reduced by treatment with Ro41-5253 (Fig. 1*B*) as well as heparin, a competitive viral attachment inhibitor that served as a positive control (Fig. 1*C*) (14). HBe in the medium (Fig. 1*D*) as well as intracellular HBc protein (Fig. 1*F*), HBV replicative (Fig. 1*G*), and cccDNA (Fig. 1*H*) were consistently decreased by treatment with Ro41-5253, without serious cytotoxicity (Fig. 1*E*). This effect of Ro41-5253 was not limited to infection of HepaRG cells because we observed a similar anti-HBV effect in primary human hepatocytes (Fig. 1*I*). The anti-HBV effect of Ro41-5253 on HBV infection of primary human hepatocytes was also observed in the absence of PEG8000 (Fig. 1*J*), which is frequently used to enhance HBV infectivity *in vitro* (14, 29). These data suggest that Ro41-5253 treatment decreases hepatocyte susceptibility to HBV infection.

Reduced HBV Entry in Ro41-5253-treated Cells—Ro41-5253 decreased HBs secretion from infected cells in a dose-dependent manner without significant cytotoxicity (Fig. 2*A*). We next investigated which step in the HBV life cycle was blocked by Ro41-5253. The HBV life cycle can be divided into two phases as follows: 1) the early phase of infection, including attachment, internalization, nuclear import, and cccDNA formation, and 2) the following late phase representing HBV replication that includes transcription, pregenomic RNA encapsidation, reverse transcription, envelopment, and virus release (19, 20, 30–34). LMV and ETV, inhibitors of reverse transcriptase, dramatically decreased HBV DNA in HepAD38 cells (Fig. 2*B*, *left panel*), which can replicate HBV DNA but are resistant to infection (22). However, LMV and ETV did not show a significant effect in HepaRG-based infection (Fig. 1*A*), in contrast to the anti-HBV effect of CsA, an HBV entry inhibitor (Fig. 2*C*) (19, 35), suggesting that this infection assay could be used to evaluate the early phase of infection without the replication process, including the reverse transcription. Ro41-5253 was suggested to inhibit the early phase of infection prior to genome replication as an anti-HBV activity was evident in Fig. 2*C* but not in Fig. 2*B*. Moreover, Ro41-5253 had little effect on HBV transcription, which was monitored by a luciferase activity driven from the HBV enhancer I, II, and the core promoter (Fig. 2*B*, *middle panel*), and by the HBV RNA level in HepG2.2.15 cells, persistently producing HBV (Fig. 2*B*, *right panel*) (36). We then examined whether Ro41-5253 pretreatment affected viral attachment to host cells. To this end, HepaRG cells were exposed to HBV at 4 °C for 3 h, which allowed HBV attachment but not subsequent internalization (19) (Fig. 2*D*). After washing out free viruses, cell surface HBV DNA was extracted and quantified to evaluate HBV cell attachment (Fig. 2*D*). Pretreatment with Ro41-5253 significantly reduced HBV DNA attached to the cell surface, as did heparin (Fig. 2*D*). In a preS1 binding assay, where FITC-labeled preS1 lipopeptide was used as a marker for HBV attachment to the cell surface, Ro41-5253-

tapraid4/zbc-bc/zbc01115/zbc0943-15z ZSUBMIT 5 xppws S=6 19/1/15 9:46 | 4/Color Figure(s) F1–3,8,9 | ARTNO: M114.602540

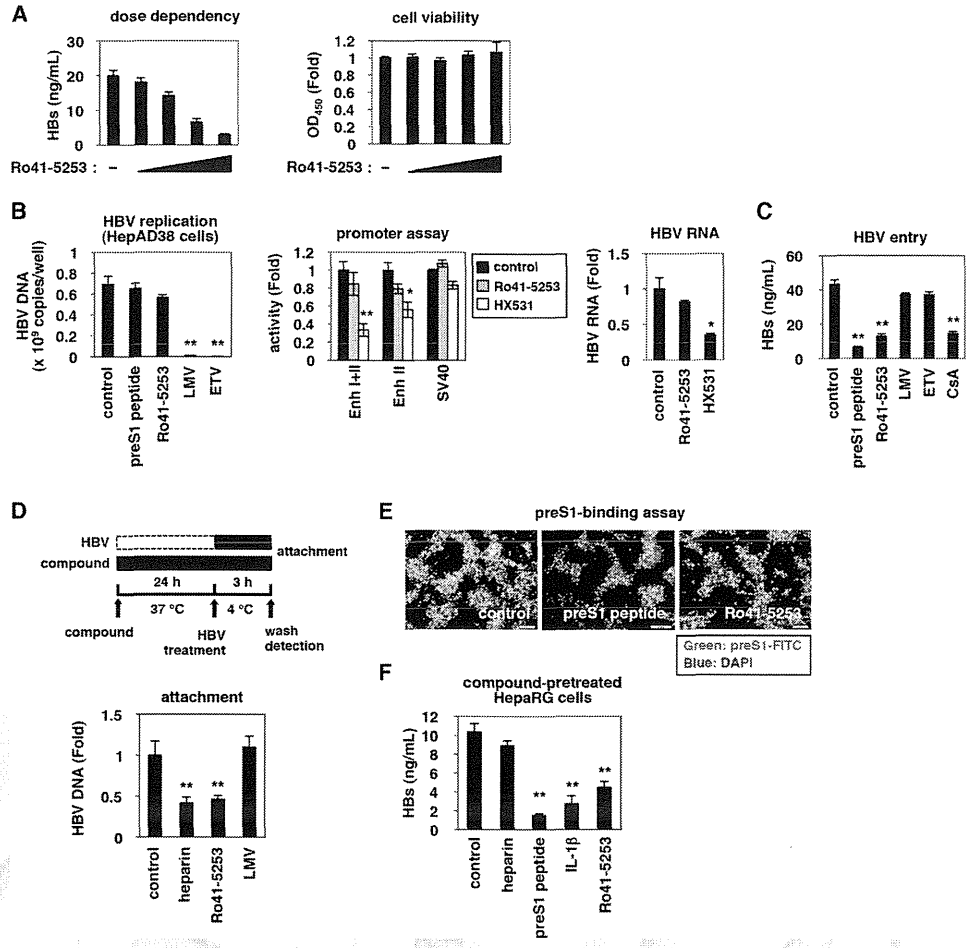

FIGURE 2. **Ro41-5253 decreased HBV entry.** *A*, HepaRG cells were treated with or without various concentrations (2.5, 5, 10, and 20 μM) of Ro41-5253 followed by HBV infection according to the protocol shown in Fig. 1*A*. Secreted HBs was detected by ELISA (*left panel*). Cell viability was also determined by ELISA (*right panel*). *B, left panel,* nucleocapsid-associated HBV DNA in HepAD38 cells treated with the indicated compounds (200 nM preS1 peptide, 20 μM Ro41-5253, 1 μM lamivudine, or 1 μM entecavir) for 6 days without tetracycline was quantified by real time PCR. *Middle panel,* HepG2 cells transfected with the reporter plasmids carrying HBV Enhancer (*Enh*) I + II, HBV Enhancer II, or SV40 promoter ("Experimental Procedures") were treated with or without Ro41-5253 or HX531 as a positive control to measure the luciferase activity. *Right panel,* HepG2.2.15 cells were treated with or without Ro41-5253 or HX531 for 6 days, and intracellular HBV RNA was quantified by real time RT-PCR. *C,* HepaRG cells were treated with or without indicated compounds (200 nM preS1 peptide, 20 μM Ro41-5253, 1 μM lamivudine, 1 μM entecavir, or 4 μM CsA) followed by HBV infection according to the protocol shown in Fig. 1*A*. *D, upper scheme* shows the experimental procedure for examining cell surface-bound HBV. The cells were pretreated with compounds (50 units/ml heparin, 20 μM Ro41-5253, or 1 μM lamivudine) at 37 °C for 24 h and then treated with HBV at 4 °C for 3 h to allow HBV attachment but not internalization into the cells. After removing free virus, cell surface HBV DNA was extracted and quantified by real time PCR. *E,* HepaRG cells pretreated with the indicated compounds (1 μM unconjugated preS1 peptide, 20 μM Ro41-5253) for 24 h were treated with 40 nM FITC-conjugated pre-S1 peptide (*FITC-preS1*) in the presence of compounds at 37 °C for 30 min. *Green* and *blue signals* show FITC-preS1 and nuclear staining, respectively. *F,* HepaRG cells pretreated with the indicated compounds (50 units/ml heparin, 200 nM preS1 peptide, 100 ng/ml IL-1β, or 20 μM Ro41-5253) for 24 h were used for the HBV infection assay, where HBV was inoculated for 16 h in the absence of the compounds. Statistical significance was determined using Student's *t* test (*, $p < 0.05$, and **, $p < 0.01$).

treated cells showed a reduced FITC fluorescence measuring viral attachment (Fig. 2*E*). Thus, Ro41-5253 primarily decreased the entry step, especially viral attachment. Next, to examine whether Ro41-5253 targeted HBV particles or host cells, HepaRG cells pretreated with compounds were examined for susceptibility to HBV infection in the absence of compounds (Fig. 2*F*). As a positive control, HBV infection was blocked by pretreatment of cells with an NTCP-binding lipopeptide, preS1(2–48)^{myr} (preS1 peptide) (15), but not by heparin, which binds HBV particles instead (Fig. 2*F*, *2nd* and *3rd lanes*) (14). HBV infection was also diminished in HepaRG cells pretreated with IL-1β, which induced an innate immune response (Fig. 2*F*, *4th lane*) (37). In this experiment, Ro41-5253-pretreated HepaRG cells were less susceptible to HBV infection (Fig. 2*F*, *5th lane*), suggesting that the activity of Ro41-5253 in host cells contributed to the inhibition of HBV entry.

Ro41-5253 Down-regulated NTCP—Next, we examined how treatment of hepatocytes with Ro41-5253 decreased HBV susceptibility. Recently, NTCP was reported to be essential for HBV entry (15). Intriguingly, we found that Ro41-5253 decreased the level of NTCP protein in HepaRG cells (Fig. 3*A*). Flow cytometry showed that NTCP protein on the cell surface was consistently down-regulated following treatment with Ro41-5253 (Fig. 3*B*, compare *red* and *blue*). Semi-quantitative RT-PCR revealed that mRNA levels for *NTCP*, but not apical sodium-dependent bile salt transporter (ASBT, also known as NTCP2 or SLC10A2), another SLC10 family transporter, were reduced by Ro41-5253 in HepaRG cells (Fig. 3*C*). Thus, Ro41-5253 could reduce NTCP expression. When endogenous NTCP and RAR was knocked down by siRNA, the anti-HBV effect of Ro41-5253 was significantly diminished (Fig. 3*D*), suggesting that the inhibitory activity of Ro41-5253 to HBV infec-

Retinoids Reduced HBV Susceptibility by Down-regulating NTCP

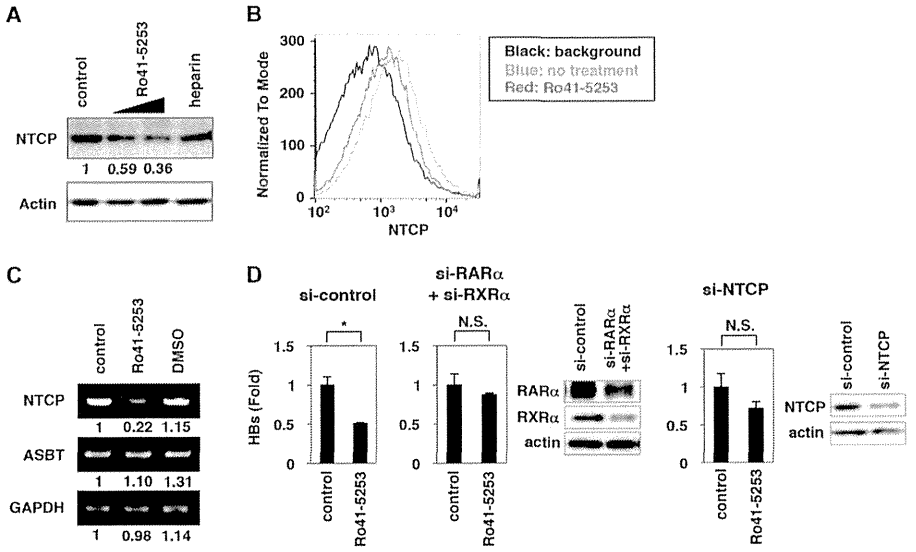

FIGURE 3. **Ro41-5253 reduced NTCP expression.** *A*, HepaRG cells were treated or untreated with 10 and 20 μM Ro41-5253 or 50 units/ml heparin for 12 h, and the levels of NTCP (*upper panel*) and actin (*lower panel*) were examined by Western blot analysis. The relative intensities for the bands of NTCP measured by densitometry are shown below the *upper panel*. *B*, flow cytometric determination of NTCP protein level on the cell surface of primary human hepatocytes treated with 20 μM Ro41-5253 (*red*) for 24 h or left untreated (*blue*). The *black line* indicates the background signal corresponding to the cells untreated with the primary antibody. *C*, RT-PCR determination of the mRNA levels for *NTCP* (*upper panel*), *ASBT* (*middle panel*), and *GAPDH* (*lower panel*) in cells treated with 20 μM Ro41-5253 or 0.1% DMSO for 12 h or left untreated. The relative intensities for the bands measured by densitometry are shown *below the panels*. *D*, HepaRG cells were treated with siRNA against RARa (*si-RARa*) plus that against RXRa (*si-RXRa*), that against NTCP (*si-NTCP*), and a randomized siRNA (*si-control*) for 3 days and then were re-treated with siRNAs for 3 days. The cells were pretreated with or without Ro41-5253 for 24 h and then infected with HBV for 16 h. HBs antigen produced from the infected cells were measured at 12 days postinfection. Statistical significance was determined using Student's *t* test (*, $p < 0.05$; *NS*, not significant).

tion was, at least in part, mediated by targeting NTCP. These data suggest that Ro41-5253 down-regulated NTCP, which probably contributed to the anti-HBV activity of Ro41-5253.

Retinoic Acid Receptor Regulated NTCP Promoter Activity—To determine the mechanism for Ro41-5253-induced down-regulation of NTCP, we used a reporter construct inserting nucleotides (nt) −1143 to +108 of the human *NTCP* (h*NTCP*) promoter upstream of the Gluc gene (Fig. 4*A*, *upper panel*). Ro41-5253 dose-dependently decreased the luciferase activity driven from this promoter, although the effect was modest and showed up to ~40% reduction (Fig. 4*A*, *left panel*). Ro41-5253 had little effect on the herpes simplex virus thymidine kinase promoter (Fig. 4*A*, *right panel*), suggesting that Ro41-5253 specifically repressed hNTCP promoter activity. As reported previously (38), Ro41-5253 specifically inhibited RAR-mediated transcription (Fig. 4, *B* and *C*). RARα, RARβ, and RARγ are members of the nuclear hormone receptor superfamily, which are ligand-activated transcription factors that regulate the transcription of specific downstream genes by binding to the RAR-responsive element (RARE) predominantly in the form of a heterodimer with RXR. We therefore asked whether RAR could regulate the h*NTCP* promoter. As shown in Fig. 4*D*, hNTCP promoter activity was stimulated by overexpression of either RARα, RARβ, or RARγ together with RXRα, and transcription augmented by RAR could be repressed by Ro41-5253 (Fig. 4*D*). Knockdown of endogenous RARα, RXRα, or both dramatically impaired the activity of the h*NTCP* promoter (Fig. 4*E*). These results suggest that RAR/RXR is involved in the transcriptional regulation of the h*NTCP* gene. Consistently, an RAR agonist, ATRA, induced *NTCP* mRNA expression (Fig. 4*F*).

Importantly, endogenous expression of RARα was more abundant in differentiated HepaRG cells, which are susceptible to HBV infection, than that in undifferentiated HepaRG and HepG2 cells, which are not susceptible (Fig. 4*G*) (29). This expression pattern was consistent with the expression of NTCP and with HBV susceptibility, suggesting the significance of RAR in regulating NTCP expression.

Promoter Analysis of hNTCP—We next examined whether RAR regulation of the h*NTCP* promoter is direct or indirect. From the analyses so far using the rat *Ntcp* (r*Ntcp*) promoter, one of the major regulators for rNtcp expression is farnesoid X receptor (FXR), which is a nuclear receptor recognizing bile acids (39). FXR, which is activated upon intracellular bile acids, indirectly regulates r*Ntcp* expression; FXR induces its downstream small heterodimer partner (Shp), another nuclear receptor, and Shp recruits to the r*Ntcp* promoter to repress the promoter activity (39). Then we examined whether RAR affected the expression of human SHP. As shown in Fig. 5*A*, F5 although an FXR agonist GW4064 remarkably induced SHP expression as reported (39), RAR did not have a remarkable effect on the SHP level in HepaRG cells (Fig. 5*A*). To assess the direct involvement of RAR in h*NTCP* regulation, the ChIP assay showed that RAR was associated with the h*NTCP* promoter both in the presence and absence of ATRA (Fig. 5*B*), consistent with the characteristic that RAR/RXR binds to RARE regardless of ligand stimulation (40). The Genomatix software predicts that the h*NTCP* promoter possesses five putative RAREs in nt −1143 to +108 (Fig. 5*C*). Introduction of mutations in all of these five elements lost the promoter activation by RAR/RXR overexpression (Fig. 5*C*, *5-Mut*). Although the promoters mutated in the motif nt −491 to −479, −368 to −356, −274 to −258, or −179 to −167 were activated by ectopic expression of RAR/RXR and this activation was cancelled by Ro41-5253 treatment, the h*NTCP* promoter with

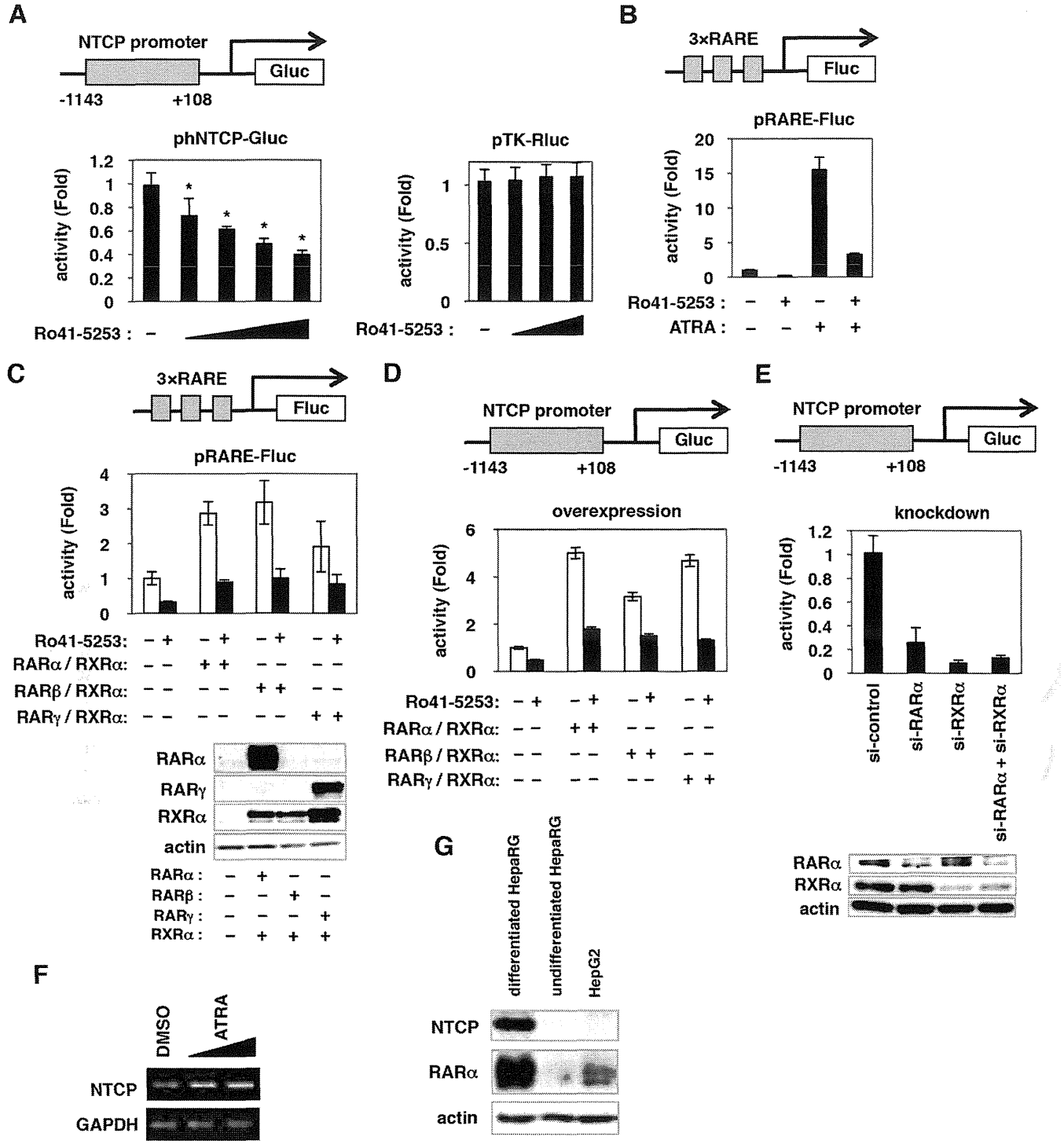

FIGURE 4. **RAR could regulate h*NTCP* promoter activity.** *A, left panel,* HuS-E/2 cells were transfected for 6 h with an hNTCP reporter construct with −1143/+108 of the h*NTCP* promoter region cloned upstream of the Gluc gene (*upper panel, phNTCP-Gluc*), together with an internal control plasmid expressing SEAP (pSEAP). Cells were treated or untreated with various concentrations of Ro41-5253 (5–40 μM) for 48 h. The Gluc and SEAP activities were determined, and the Gluc values normalized by SEAP are shown. *Right panel,* HuS-E/2 cells transfected with a reporter construct carrying the herpes simplex virus thymidine kinase promoter (*pTK-Rluc*) were examined for luciferase activity in the presence or absence of Ro41-5253 (10–40 μM). *B,* HuS-E/2 cells transfected with a Fluc-encoding reporter plasmid carrying three tandem repeats of RARE (*upper panel, pRARE-Fluc*), and Rluc-encoding reporter plasmid driven from herpes simplex virus thymidine kinase promoter (*pTK-Rluc*) were treated with or without 20 μM Ro41-5253 in the presence or absence of an RAR agonist, ATRA, 1 μM for 24 h. Relative values for Fluc normalized by Rluc are shown. *C,* HuS-E/2 cells transfected with pRARE-Fluc and pTK-Rluc with or without expression plasmids for RARs (RARα, RARβ, or RARγ) and RXRα were treated with (*black*) or without (*white*) Ro41-5253 for 48 h. Relative values for Fluc/Rluc are shown. *D,* HuS-E/2 cells were cotransfected with phNTCP-Gluc and pSEAP with or without the expression plasmids for RARs (RARα, RARβ, or RARγ) and RXRα, followed by 24 h of treatment or no treatment with 20 μM Ro41-5253. Relative Gluc/SEAP values are shown. *E,* phNTCP-Gluc and pSEAP were transfected into HuS-E/2 cells together with siRNAs against RARα (*si-RARα*), RXRα (*si-RXRα*), si-RARα plus si-RXRα, or randomized siRNA (*si-control*) for 48 h. Relative Gluc/SEAP values are indicated. Endogenous RARα, RXRα, and actin proteins were detected by Western blot analysis (*lower panels*). *F,* mRNA levels for *NTCP* and *GAPDH* were detected in differentiated HepaRG cells treated with or without ATRA (0.5 and 1 μM) for 24 h. *G,* protein levels for endogenous NTCP (*upper panel*), RARα (*middle panel*), and actin (*lower panel,* as an internal control) were determined by Western blot analysis of differentiated HepaRG, undifferentiated HepaRG, and HepG2 cells. Statistical significance was determined using Student's *t* test (*, $p < 0.05$).

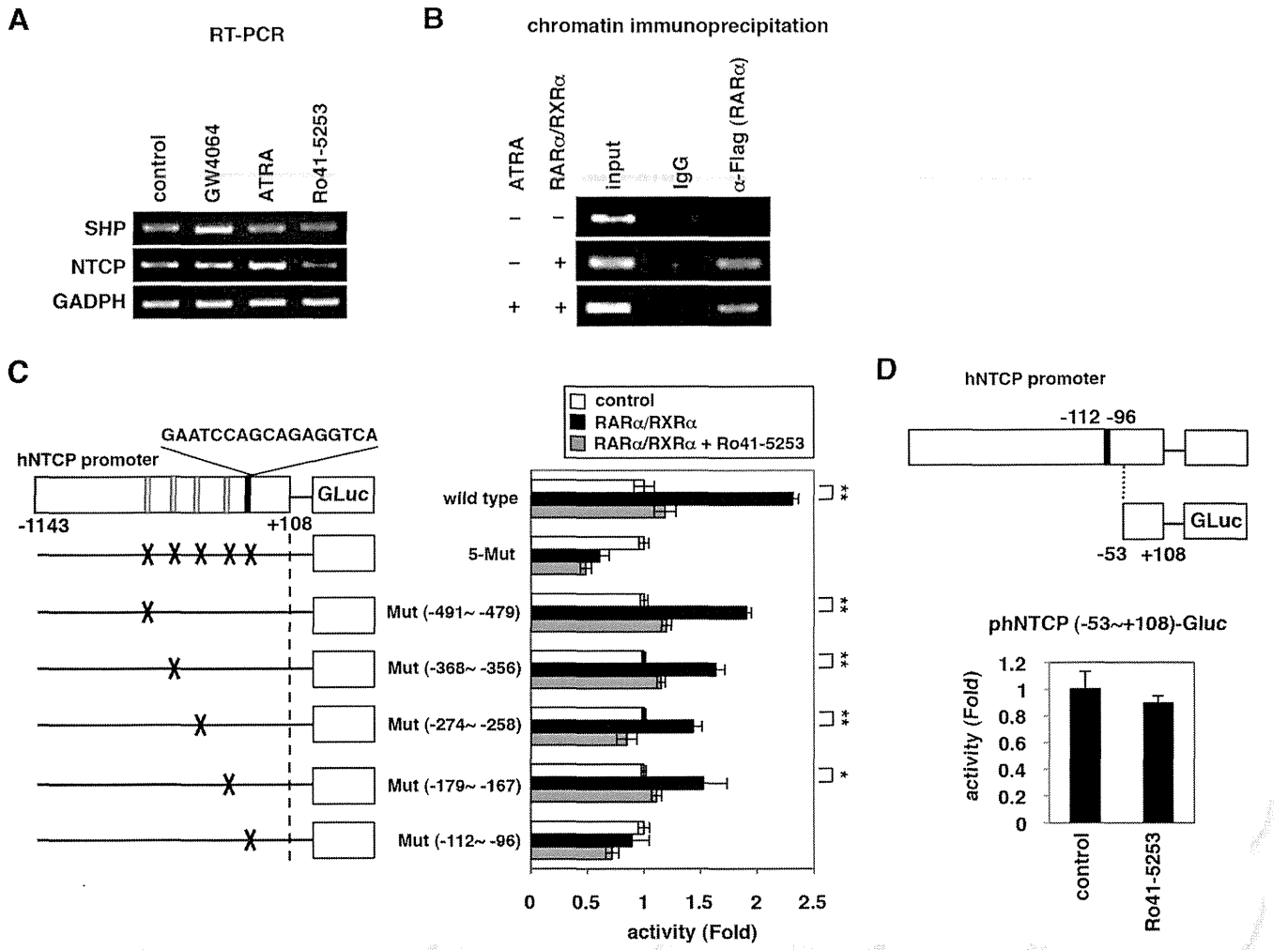

FIGURE 5. **RAR directly regulated the activity of hNTCP promoter.** *A*, HepaRG cells were treated with or without ATRA, Ro41-5253, or a positive control GW4064, which is an FXR agonist, for 24 h. mRNAs for SHP as well as *NTCP* and *GAPDH* were detected by RT-PCR. *B*, ChIP assay was performed as described under "Experimental Procedures" with Huh7-25 cells transfected with or without an expression plasmid for FLAG-tagged RARa plus that for RXRa in the presence or absence of ATRA stimulation. *C*, *left panel*, schematic representation of h*NTCP* promoter and the reporter constructs used in this study. h*NTCP* promoter has five putative RAREs (nt −491 to −479, −368 to −356, −274 to −258, −179 to −167 (*gray regions*), and −112 to −96 (*black regions*, GAATCCAGCAGAGGTCA)) in nt −1143 to +108 of h*NTCP*. The mutant constructs possessing mutations within each putative RAREs and in all of five elements (*5-Mut*) as well as the wild type construct are shown. *Right panel*, relative luciferase activities upon overexpression with or without RARa plus RXRa in the presence or absence of Ro41-5253. *D*, deletion reporter construct carrying the region nt −53 to +108 of the h*NTCP* upstream of the Gluc gene was used for the reporter assay in the presence or absence of Ro41-5253.

mutations in nt −112 to −96 had no significant response by RAR/RXR (Fig. 5*C*). These data suggest that the nt −112 to −96 region is responsible for RAR-mediated transcriptional activation of h*NTCP*.

HBV Susceptibility was Decreased in RAR-inactivated Cells—We further investigated the impact of RAR antagonization on HBV infectivity. BMS195614, BMS493, and MM11253, which repressed RAR-mediated transcription (Fig. 6*A*), all decreased the susceptibility of HepaRG cells to HBV infection (Fig. 6*B*) without significant cytotoxicity (Fig. 6*C*). These data confirmed that HBV infection was restricted in RAR-inactivated cells. Among these, CD2665, a synthetic retinoid that is known to inhibit RAR-mediated transcription (Fig. 7*A*), had more potent anti-HBV activity than Ro41-5253 (Fig. 7*B*), which was accompanied by the inhibition of the hNTCP promoter (Fig. 7*C*) and down-regulation of NTCP protein (Fig. 7*D*).

CD2665 Showed a Pan-genotypic Anti-HBV Effect—We then examined the effect of CD2665 on the infection of primary human hepatocytes with different HBV genotypes. CD2665 significantly reduced the infection of HBV genotypes A, B, C, and D, as revealed by quantification of HBs and HBe antigens in the culture supernatant of infected cells (Fig. 8, *A–D*). Additionally, this RAR inhibitor decreased the infection of the ETV- and LMV-resistant HBV genotype C clone carrying mutations in L180M, S202G, and M204V (Fig. 8, *E* and *F*). Thus, CD2665 showed pan-genotypic anti-HBV effects and was also effective on an HBV isolate with resistance to nucleoside analogs. F8

We further investigated whether RAR inhibitors could prevent HBV spread. It was recently reported that HBV infection in freshly isolated primary human hepatocytes could spread during long term culture through production of infectious virions and reinfection of surrounding cells (41). As shown in Fig. 8*G*, the percentage of HBV-positive cells increased up to 30 days postinfection without compound treatment (Fig. 8*G*, *panels a–d*). However, such HBV spread was clearly interrupted by treatment with Ro41-5263 and CD2665 as well as preS1 peptide AQ: A